

High-entropy alloys as an alternative binder to improve mechanical, tribological, and oxidation properties of cermets

Madrid, C.; Cáceres, C.; Jiménez-Arévalo, Víctor M.; Martín, P.; Araya, N.; Aguilar, C.

DOI

[10.1016/j.matdes.2024.113431](https://doi.org/10.1016/j.matdes.2024.113431)

Publication date

2024

Document Version

Final published version

Published in

Materials and Design

Citation (APA)

Madrid, C., Cáceres, C., Jiménez-Arévalo, V. M., Martín, P., Araya, N., & Aguilar, C. (2024). High-entropy alloys as an alternative binder to improve mechanical, tribological, and oxidation properties of cermets. *Materials and Design*, 247, Article 113431. <https://doi.org/10.1016/j.matdes.2024.113431>

Important note

To cite this publication, please use the final published version (if applicable). Please check the document version above.

Copyright

Other than for strictly personal use, it is not permitted to download, forward or distribute the text or part of it, without the consent of the author(s) and/or copyright holder(s), unless the work is under an open content license such as Creative Commons.

Takedown policy

Please contact us and provide details if you believe this document breaches copyrights. We will remove access to the work immediately and investigate your claim.



High-entropy alloys as an alternative binder to improve mechanical, tribological, and oxidation properties of cermets

C. Madrid ^a, C. Cáceres ^a, Víctor M. Jiménez-Arévalo ^b, P. Martin ^{c,d,*}, N. Araya ^e, C. Aguilar ^a

^a Departamento de Ingeniería Metalúrgica y de Materiales, Universidad Técnica Federico Santa María, Valparaíso, Chile

^b Departamento de Química de los Materiales, Facultad de Química y Biología, Universidad de Santiago de Chile, Av. B. O'Higgins 3363, Santiago, Chile

^c Department of Materials Science and Engineering, Delft University of Technology, Delft, Netherlands

^d Department of Materials Science and Engineering, Universitat Politècnica de Catalunya-BarcelonaTech, Barcelona, Spain

^e Departamento de Ciencia e Ingeniería de Materiales, Universidad de Concepción, Concepción, Chile

ARTICLE INFO

Keywords:

High-entropy alloys

Cermets

Cemented carbides

Complex composition alloys

ABSTRACT

Due to elevated potential associated with the extremely vast compositional space of high-entropy alloys (HEAs), there is a significant drive to explore these alloys in high-performance contexts such as intensive wear and oxidative environments. In this regard, this review article comprehensively explores the utilization of HEAs in cemented carbides, focusing on their role as binders in cermets. The wear resistance and oxidation behavior of HEA-containing cermets depends on the ceramic-binder thermodynamic compatibility, phase transformations during sintering, microstructure, and mechanical properties. Hence, much high quality research has been focused into exploring the combination of several HEAs with tungsten carbide, titanium carbides, nitrides, carbonitrides and diborides along with other ceramic compounds. As there are many HEA-ceramic combinations, this review aims to provide a landscape of the developments in this field, providing detailed information about the chemical compositions, sintering techniques, mechanical properties and wear and oxidation resistance obtained. Finally, the need for further research to fully understand the complex interactions between composition, microstructure, and wear and oxidation resistance is highlighted, aiming to tailor HEA compositions for optimized performance. The findings presented in this review contribute valuable insights into the promising applications of HEAs in cemented carbides.

1. Introduction

Cemented carbides, are ceramic/metal composites used in cutting tools whose performance is situated between that of cermets and tool steels; hence, these are harder and more wear resistant than the latter but with lower toughness and thermal conductivity [1]. The first marketable cemented carbide (commonly referred to as “Straight grade”) was invented in 1923 by Karl Schröeter at Osram Studiengesellschaft, Germany [2–4]. The compound consisted of WC particles bonded with Co as the binder phase [1] and was first used to replace diamond in extruder nozzle tips to produce W filaments used in incandescent bulbs. Global production of WC-Co based hardmetals has grown rapidly over the last 30 years, with total production of approximately 20,000 ton/year in 1993 and increasing to over 60,000 ton/year with China’s entry into the market in 2008 [5]. 65 % of the world’s production goes to the manufacture of cutting tools, approximately 15 %

corresponds to the mining, oil and rock excavation industry, about 11 % belongs to the woodworking industry and, finally, the construction industry accounts for the remaining 9 % of the market share [1,5]. Thus, the worldwide market for WC-Co hard metals comprises approximately 50 % compared to other cutting tools (i.e. high speed steels (HSS), Boron Nitrides, TiN, etc.) [2,5,6].

For wear related applications, the microstructure of cermets consists of a ceramic phase, characterized by high hardness, elastic modulus and wear resistance, bonded with a metallic matrix that imparts toughness and ductility to the alloy [1,2,7]. The binder phase content in commercially significant cemented carbides varies from 2 to 30 wt% [1,3]. For conventional WC – Co, their mechanical properties vary with the binder content, so their hardness can range from ~6.9 to 35.3 GPa (~700 to 3600 HV), while their the modulus of elasticity (E) and compressive strength ranges between 400–700 GPa and 300–9000 MPa, respectively [3,5]. However, they are characterized by a low fracture

* Corresponding author at: Department of Materials Science and Engineering, Delft University of Technology, Delft, Netherlands.

E-mail address: p.m.martinsaint-laurence@tudelft.nl (P. Martin).

<https://doi.org/10.1016/j.matdes.2024.113431>

Received 10 August 2024; Received in revised form 29 October 2024; Accepted 3 November 2024

Available online 5 November 2024

0264-1275/© 2024 The Authors. Published by Elsevier Ltd. This is an open access article under the CC BY license (<http://creativecommons.org/licenses/by/4.0/>).

toughness (5–30 MPa·m^{1/2}) [2,5], low resistance to corrosive environments, and poor performance at elevated temperatures [8,9]. Additionally, these cermets present thermal stresses, product of the difference between the coefficients of thermal expansion of their constituents ($\Delta\alpha \approx 6 \times 10^{-6} [K^{-1}]$), where an excess of Co has negatively influenced the thermal fatigue resistance of cermet [10,11]. In fact, these factors have led to poor performance in operation, where binder phase degradation has caused cermet failure at speeds not much higher than those used in high-speed steels [1].

The European Union has classified W and Co, among other elements, as critical raw materials, due to the difficulty of their extraction due to the lack of easily accessible deposits [12]. Furthermore, according to World Economic Forum [13], the market for lithium-ion batteries (which contain Co as one of their constituents) is expected to increase by at least 25 % each year, and the demand for Co is projected to at least quadruple by 2030, compared to last year's levels [14]. In addition, Co is considered to be a carcinogenic agent, because prolonged exposure to hard metal dust in suspension considerably increases the mortality of people due to lung cancer [15] and heart problems [16]. These problems have motivated researchers to develop new cemented carbides or cermets, with a total or partial replacement of Co as a binder and/or WC as the hard phase. Various elements (Fe, Ni, Cr, etc.), intermetallic compounds (Ni₃Al, FeAl, among others) and some ceramics (Al₂O₃, MgO) have been studied to replace the Co present in cemented carbides [17]. On the other hand, hard particles like TiC, TiN, Ti(C,N), TiB₂, FeB, NbC, etc. have been proposed to replace the WC.

The choice of Fe as the binder phase is attributed to its ability to inhibit grain growth, its non-toxicity and low price [18]. However, with the publication of the first phase diagram of the Fe-W-C ternary system by Takeda in 1936 [19], it could be observed that the alloy is prone to form the eta carbide ($\eta - M_6C$) at a stoichiometric C content of WC, due to the high affinity of Fe for C, which generates a decrease in the mechanical properties of the material. The formation of this phase was avoided with the addition of free C i.e., C that is not contained in the hard phase. However, the resulting mechanical properties were inferior to those of WC-Co [20], reaching only 40–60 % of the transverse rupture strains (TRS) of similar WC-Co composites [21]. On the other hand, Ni has been also explored as a binder aid for these cermets. The first binary binder (Fe-Ni) successfully used for the fabrication of cutting tools was developed by Agte in 1957 [22]. The good performance of these materials depends mainly on the absence of the intermetallic compound M₆C and free graphite in their microstructure [21,23]. The first Fe-Ni-W-C phase diagram was presented by Kohlermann and Wehner in 1957, followed by Gabriel in 1984 and Guillermet in 1987 [24–26], the latter being successfully used as a guide for the development of new WC/Fe-Ni alloys. The phase diagram shows that an increase in the amount of binder causes the two-phase field of interest to widen, and that by varying the Ni content (maintaining a constant binder content), an increase in Ni generates a preliminary tightening and subsequently a widening of the admissible composition range to achieve a stable two-phase structure at room temperature [24].

Mn is another element that has been used in conjunction with Fe to form part of the binder in a cemented carbide, due to its similarity with Co in terms of melting temperature, lattice structure, and phase transformation during cooling, as well as its low cost and reduced toxicity [27]. The martensitic transformation of these compounds can generate stacking faults, mainly responsible for the increase in mechanical strength and resistance to plastic flow of the binder [28], an approach supported by the research conducted by Sevost'yanova et al. [29]. Hanyaloglu et al. [27] studied the mechanical properties of two cemented carbides, WC-15(Fe-13.5Mn) and WC-25(Fe-13.5Mn), obtaining higher hardness than its alloy counterpart of WC-Co, 35.4 % y 78 %, respectively. Complementarily, the results obtained by Schubert et al. [30] show that the range of tenacity in alloys with WC-10%(Fe (2–16)Mn) ranges from 7.5 to 7.8 MPa·m^{1/2}, lower than that recorded by

its alloy counterpart of WC-Co (8.5–10 MPa·m^{1/2}).

Other elements used as alloying agents in Fe-based binders are Mn, Cu, Cr, and Mo. Mn allows obtaining harder but more brittle composites [27,30] while Cu generates a greater densification of the material and an increase in the TRS, without increasing the hardness of the material [31]. The addition of Cr suppresses the grain growth of the ceramic phase and improves the corrosion and oxidation resistance of cemented carbide [32,33]. Finally, Zhao et al. [34] determined that Mn generates an increase in TRS and prevents grain growth of the reinforcing phase, without further affecting the hardness of Fe-Ni-W-C alloys.

Aluminides such as Ni₃Al, are an attractive option for use as a binder because it has been shown to possess favorable wettability over WC [35,36], high hardness, high melting point, low density, excellent corrosion and oxidation resistance, and high elastic modulus [37,38]. Liang et al. [39] synthesized a WC-10wt.%Ni₃Al cemented carbide and determined that it exhibits better performance compared to a WC-8Co composite when cutting at high speeds. In turn, Liu et al. [40] studied the resistance of these cermets to abrasive wear, observing that WC-8Co has a lower wear resistance than the aluminide composite. The results presented are attributed to the high hardness and low chemical reactivity of the Ni₃Al.

Despite intensive efforts to obtain a comprehensive improvement of the performance and mechanical properties of WC-Co based cemented carbides, only a partial improvement of these materials has been achieved [41]. However, with the development of the firsts high-entropy alloys (HEAs), independently proposed by Cantor et al. [42] and Yeh et al. [43] in 2004, a whole new field of studies focused on the development of new cemented carbides or cermets using HEAs as binder phase was opened. HEAs were conceived as those metallic materials constituted for at least 5 elements, all of them between a 5 and 35 at. %, without a clear base element as in traditional alloys. In the liquid state, their complex composition would conduct them to a totally mixed state with an elevated ideal configurational entropy, that would stabilize a solid solution – containing all the constituent elements – even after cooling up to room temperature by means of the elevated entropic term [44]. The first HEAs effectively presented only face-centered cubic (FCC) and body-centered cubic (BCC) solid solutions, just as was hypothesized, revealing a potential new field of metallic materials.

Nevertheless, further research has revealed that single-phase solid solution microstructures in HEAs are obtained only in particular cases, and most of these alloys actually present multi-phase microstructures, containing either multiple solid solutions, or well, solid solutions accompanied by intermetallic phases; even more, single-phase intermetallic phases microstructures have been observed too. Despite the mostly multiphase character of HEAs, they have exhibited excellent combinations of properties, including high hardness [45,46], high yield stress [47,48], excellent fatigue resistance [49], good fracture toughness [50], and superior oxidation resistance [51]. All these remarkable features make these relatively new alloys ideal candidates to be used as binders in the fabrication of cermets.

Several review articles addressing the definition, composition, microstructure, and performance of HEAs can be found in literature; in this context, this work aims to discuss and analyze the development of cermets utilizing HEAs as binders, focused on the interaction between the hard phase and the HEA binder. A concise analysis of the relationship between binder composition, processing method, microstructure and mechanical, wear, and oxidation resistance are presented, in order to have a complete understanding of the potential of HEAs in these applications.

2. Microstructure, mechanical, and tribological properties of HEAs-bonded cermets

One of the main features of HEAs is the vast universe of alloys that can be classified in this category. According to Cantor et al. [42], if only 40 elements of the periodic table are considered as potential constituent

elements and taking step sizes of 1 at. %, an enormous number of 10^{36} compositions can arise. This is indeed the origin of the wide variety of potential microstructures that characterize HEAs, and more importantly, of the interesting catalogue of properties that they have to offer. In this manner, the complex composition of HEAs widens the potential interactions between binder and hard phases, which in the case of traditional alloys utilized as binders, are mostly identified and considerably reduced in number. Since the mechanical behavior and the tribological response of the cermet will be strictly associated with its microstructure – which is an outcome of the composition and fabrication route – is not possible to understand the firsts ones without considering the role that the microstructural features play.

The fabrication technique in most of the studies in the field has been limited to sintering techniques – preceded or not by milling processes – including spark plasma sintering (SPS), hot pressing (HP), hot isostatic pressing (HIP), and pressureless sintering, either in vacuum or inert atmospheres. A description of these processes can be found elsewhere [52,53], and reviews especially dedicated to the powder metallurgy fabrication of HEAs are available as well [54,55]. Nevertheless, in the specific case of HEAs cermets, the most important variables in the study of their feasibility is the composition of the binder and the hard phase, with the sintering temperature and binder content in secondary roles as well.

In this manner, for a better understanding of the topic, the current section will be divided firstly based on the hard phase, due to their characteristics determine the base features of the cermet (due to the hard phase constitutes the majority of the volume of the cermet). Since a considerable number of articles and results have been produced addressing WC-based cermets, that particular section will be subdivided based on the binder composition as well. In this manner, the particularities of the constituent elements of the binder and their interaction with the corresponding hard phase can be clearly identified, in order to establish guidelines for the future design of HEAs-cermets.

2.1. WC-based cermets

The WC-HEAs cermets are the most studied ones among cermets; even more, from the articles considered in this review, almost 50% of them are solely based on WC. Fig. 1 summarizes the hardness of WC-cermets fabricated by sintering as a function of the sintering temperature, employing different binder contents and composition. As can be appreciated, there is no straightforward effect of the sintering temperature over hardness, since this is a property that depends on several

factors beyond composition. Among them, grain size and densification are both affected by sintering temperature but in opposite manners: increasing the sintering temperature will result in a higher densification but in a coarse grain size. While the first contributes to a higher hardness, a more coarse grain size commonly results in lower hardness values. As can be observed in the Figure, the higher hardness were obtained with sintering temperatures of 1500 °C (in the cermets containing 10 wt% and 20 wt% of AlCoCrFeNiTi [56]) and 1300 °C (in the cermets containing 5 wt% and 10 wt% of CoCrFeNiMn [57]). In opposition, the three lower hardness values were reported using sintering temperatures of 1200 °C (30 wt% of CoCrCuFeNi [58]), 1300 °C (10 wt% of AlCoCrFeNi [59]) and 1400 °C (25.5 wt% of AlCoCrNiTi [60]). A complete summary of the chemical and microstructural features of WC-HEAs cermets, as well as their fabrication procedure and resultant mechanical properties in the sintered state can be found in Table S1 (Supplementary Material).

2.1.1. CoCrFeMnNi alloy

From Table S1, it can be appreciated that most of them are based in the Cantor' alloy – an equiatomic CoCrFeNiMn alloy with a face-centered cubic (FCC) single-phase solid solution, firstly reported in [42] and the most studied HEA up to the date [61]. Hence, this composition can be considered as a starting point to understand the effect of other constituent elements in the microstructure and properties of WC-HEAs cermets. Hence, Velo et al. [62] studied the binder content effect on the microstructure and hardness of the WC-CoCrFeNiMn cermet. The microstructure of all of the samples was constituted by a FCC solid solution, WC and η -carbides ((Fe,Co,Ni)₃W₃C, (Fe,Co,Ni)₆W₆C). The presence of these carbides can have a positive effect on the mechanical behavior of the material, especially regarding to the wear resistance [63]. Particularly, the sample with 30 vol% binder and WC initial particle size of 27 μ m presented a core-rim structure, shown in Fig. 2 with a core constituted by the WC carbide particles embedded in the HEA matrix (region A1 in Fig. 2(a)) and surrounded by (Fe,Co,Ni)₃W₃C in the shell (region A2 in Fig. 2(a)). This microstructure resulted in the highest hardness among the studied cermets, registering a value of 13.15 GPa in the core and 22.15 GPa in the shell.

Ruiz-Esparza-Rodriguez et al. [57,64,65] studied the effect of the binder content, sintering temperature, and sintering time on the microstructure and mechanical properties of the WC-CoCrFeNiMn cermet. In contrast to the previous, the microstructure was constituted by several oxides alongside the FCC metallic binder and WC. The highest densification (94.44 %) was achieved employing 20 wt% of the binder

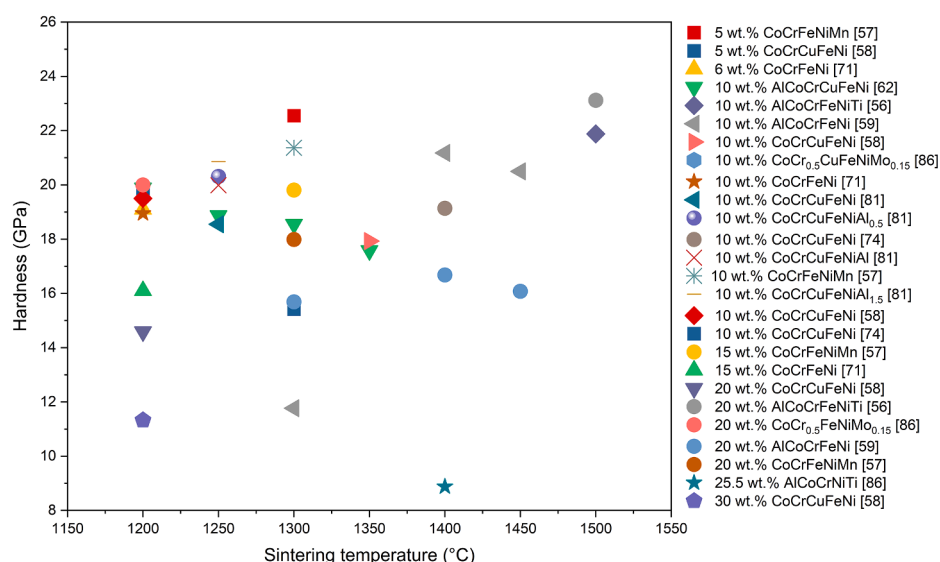


Fig. 1. Hardness as the effect of sintering temperature of WC-HEA cermets fabricated using milling followed by sintering routes.

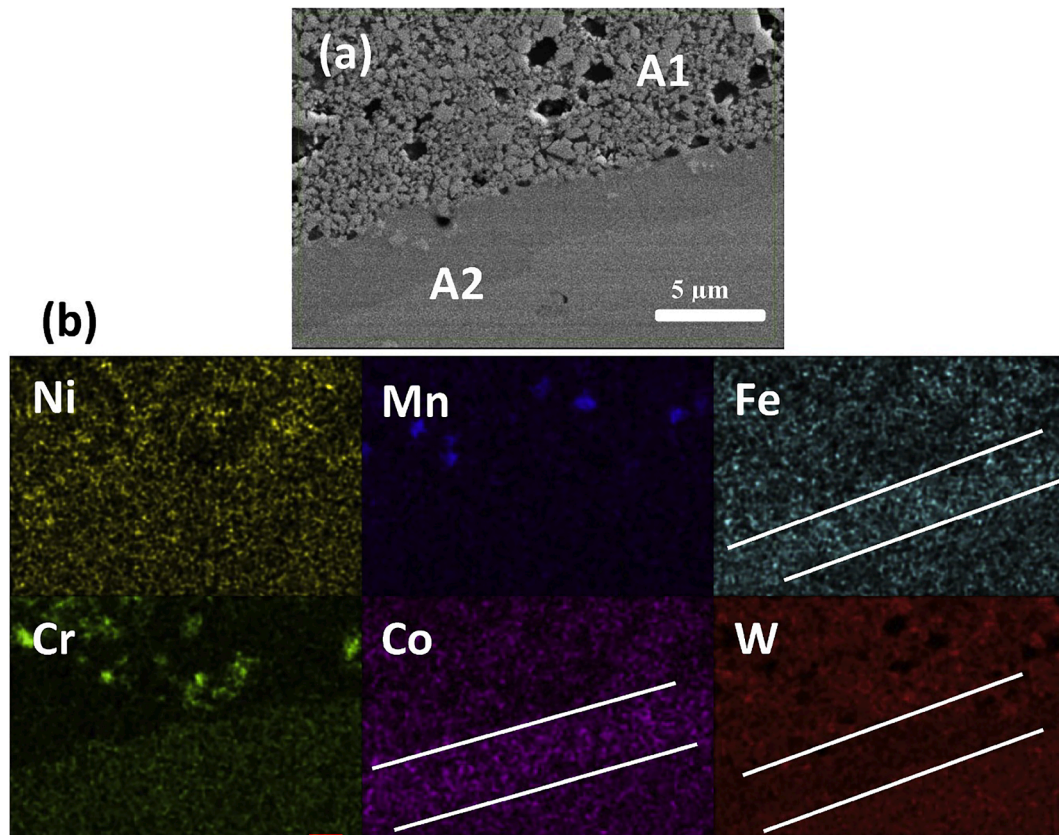


Fig. 2. (a) Characteristic SEM micrographs of WC-30 vol% FeCoCrNiMn cermet. (b) Compositional mapping of the area showing the different microstructure [62]. Reproduced with permission of Elsevier.

and sintering in vacuum at 1400 °C for 5h. Nevertheless, the highest hardness (23.24 GPa) was attained by the cermet with 5 wt% of binder, sintered in vacuum at 1300 °C by 5h; this, however, presented an elevated remanent porosity (~10 %) that could be detrimental for the composite performance.

An alternative strategy employing a mixture of CoCrFeNiMn and Co as a binder was taken by Dong et al. [66], studying both the effect of binder content (10 % to 20 %) and the binder Co/HEA ratio (4:0 to 0:4) on the microstructure and mechanical properties of the cermets. The microstructure of the samples was composed by an FCC solid solution, WC, and Co that increasingly dissolved C and the HEA as the sintering process proceeds. Besides, when the CoCrFeNiMn content was over 5 wt %, η -carbides (M_3W_3C) were observed at the WC-FCC solid solution

interface due to their interaction. On the other hand, a high presence of pores were observed, as well as a lower Mn content was measured in the FCC solid solution, indicating its sublimation during the liquid phase sintering. Hence, the highest Vickers hardness (~ 9.8 GPa) was achieved using 5 wt% Co + 5 wt% HEA as binder phase, very similar to that reported in [60,67,68] with the WC-CoCr_{0.1}Fe_{0.1}Ni_{0.8} cermet. Apart from the low hardness, a low fracture toughness (6.4 Mpa·m^{1/2}) was reported, attributed to both the high remanent porosity and the η -carbides presence. An increase of the binder content up to 10 wt% Co + 10 wt% CoCrFeNiMn increases this value to 17.8 Mpa·m^{1/2}, slightly decreasing its hardness. Hence, this article reveals some of the difficulties that can be faced employing HEAs as binders for WC cermets.

Ruiz-Esparza-Rodriguez et al. [64] studied the effect of binder

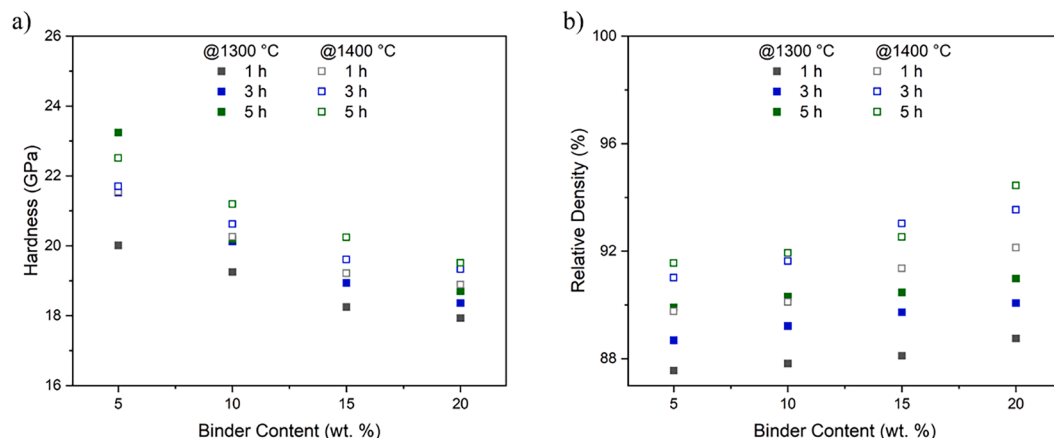


Fig. 3. Effect of the binder content, sintering time, and sintering temperature over densification and hardness of the WC-CoCrFeMnNi cermet [64].

content, sintering time, and sintering temperature over densification and hardness of the WC-CoCrFeMnNi cermet. The results are summarized in Fig. 3. As can be appreciated, increasing the binder content results in a monotonical reduction of hardness and increase in densification. Nonetheless, the effect of sintering conditions is not as simple as expected: the maximum hardness is found in the WC-5 wt.%CoCrFeMnNi after 5h of sintering at 1300 °C rather than at 1400 °C, nonetheless this latter presented a higher densification than the first. Since the authors did not perform an exhaustive characterization of the microstructure of the sintered samples, it is not possible to establish the reasons behind this peculiar tendency.

2.1.2. CoCrFeNi system

Following the previous, and dispensing of Mn, the Co-Cr-Fe-Ni system has been employed in several reports [60,68–71]. Despite the equiatomic CoCrFeNi can be considered as a medium-entropy alloy binder, in the present review it will be referred as a HEA for simplicity. Zheng et al. [71], studying the equiatomic CoCrFeNi HEA as binder, reported that the cermet was composed exclusively of a FCC solid solution and WC phases. According to the authors, an increment in the binder content (from 6 to 15 wt%) straightforwardly decreased the hardness (from 19.1 GPa to 16.1 GPa) and increased the fracture toughness (11.7 MPa·m^{1/2} to 16.8 MPa·m^{1/2}). The best results were reported by employing an intermediate 10 wt% of binder (18.95 GPa and 15.88 MPa·m^{1/2}), even superior to those of the WC-10 wt.%Co (16.98 GPa and 14.76 MPa·m^{1/2}) fabricated under the same conditions. Meanwhile the better fracture toughness was attributed to the intrinsic superior ductility of FCC structures (attained with the HEA) in comparison to that of the HCP lattice structure of Co, the higher hardness levels can be attributable to the multi-element solid-solution has a higher hardness than elemental Co and the smaller WC-grains. On the other hand, the high softening resistance of the WC-CoCrFeNi composite is mainly attributed to the diffusion retardation effect, directly related to the delayed densification of the HEA specimen. Soria-Biurrún et al. [60] also reported a FCC binder+WC microstructure in the WC-15wt.%CoCrFeNi, as long as the C content is maintained within the C window – that is, the C range in which no precipitation of either graphite or secondary carbides is observed.

Further investigation on the Cr and C effect on the microstructure and C window of WC-CoCrFeNi cermet was performed by Soria-Biurrún et al. [69]. Since Cr possess a BCC stabilizing effect, the addition of 0.75 wt% of Cr to the binder composition modifies the binder microstructure from fully FCC to a mixture of FCC + BCC. Nevertheless, if the Cr content is at least 0.75 wt% and the C content exceeds the C window, the precipitation of the brittle M₇C₃ carbide is observed. Similarly, Qian et al. [67,68] investigated the effect of C, Fe and Ni content on the C window and microstructure of WC-20wt.%CoNi_{0.8}Cr_{0.1}Fe_{0.1} and WC-20wt.%CoNi_{0.7}Fe_{0.2}Cr_{0.1} cermets. The C window became wider with Ni additions and narrower with Fe additions, noticing that the lower limit is higher in WC-HEAs cermets (4.7–4.9 wt% C) rather than in WC-Co cermets. Both cermets were composed by an FCC binder, WC ceramic phase, M₇C₃ and (W, Cr)C, reducing the interfacial energy and stress concentration. During the dissolution-precipitation process of the WC particles during the sintering process, the (W, Cr)C phase formed in the WC/HEA interface exerts a pinning effect on the WC moving boundaries. During the dissolution process, the W and C atoms must first diffuse through the (W, Cr)C layer into the binder, and, during the re-precipitation process, both atoms again need to diffuse through the (W, Cr)C layer onto the growing WC grain. Therefore, as compared to WC-Co (WC grain size: 1.82 μm; MFP: 1.63 μm), the WC- 20 wt.%CoNi_{0.7}Fe_{0.2}Cr_{0.1} exhibited a lower WC grain size (1.46 μm) and a larger mean free path (1.78 μm).

2.1.3. Cu-containing CoCrFeNi system

The microstructure and performance of WC-CuCoCrFeNi cermets have been studied as well by several authors [58,72–74], exploring

different C, Co or binder contents. Zou et al. [58] determined that an increase in the binder content (between 5 and 30 wt%) did not produced changes in the phase equilibrium, since a mixture of WC + FCC phases was observed in all the cases. Nonetheless, it did produce a gradually reduction of the WC grain size as well as of the Vickers hardness, evolving from 19.78 GPa and 472 nm, to 11.33 GPa and 286 nm, respectively. A binder content of 10 wt% lead to the maximum densification (98.7 %) as well as to an attractive combination of hardness, fracture toughness, and RT compressive strength (19.5 GPa, 10.98 MPa·m^{1/2}, and 3307 MPa, respectively). The tribological response of the WC-10wt.%CoCrCuFeNi cermet under different conditions (load, velocity, temperature and testing time) was investigated by Zou et al. [72] using a pin-on-disk configuration with a #45 steel disk (50 HRC), results are summarized in Fig. 4. As observed in Fig. 4(a), the increase in testing load from 200 to 400N while maintaining the velocity and time, resulted in a decrement of the coefficient of friction (COF) from 0.692 to 0.45 (38.44 %), while the wear rate (WR) gradually increased from 8.17×10⁻⁷ mm³·N⁻¹·m⁻¹ to 9.8×10⁻⁷ mm³·N⁻¹·m⁻¹ (20 %). Similarly, Fig. 4(b) shows that an increasing the testing speed from 0.12 m/s to 0.36 m/s at a constant load of 300N for 10 min, reduced the COF from 0.622 to 0.514 (~17 %) and increased the WR from 8.68×10⁻⁷ mm³·N⁻¹·m⁻¹ to 8.89×10⁻⁷ mm³·N⁻¹·m⁻¹ (~2.5 %). The increment of testing time from 10 min to 1h slightly increases the COF in 3.38 % and further increases the WR in ~6 %, as depicted in Fig. 4(c). Finally, an increase in testing temperature from ambient temperature to 500°C (as shown in Fig. 4(d)) considerably reduces the COF from 0.514 to 0.365 and increases the WR from 8.89×10⁻⁷ mm³·N⁻¹·m⁻¹ to 11.2×10⁻⁷ mm³·N⁻¹·m⁻¹ (26 %). The best performance was achieved applying a load of 300N and a velocity of 0.36 m/s at RT, reporting a COF of 0.514 and a WR of 8.89×10⁻⁷ mm³·N⁻¹·m⁻¹. An excellent high-temperature was observed by raising the temperature up to 500 °C, that caused a reduction of the COF in a 29 % and a raise in the WR in 25 %, as well as absence of oxides.

The effect of Co content and the sintering temperature in the WC-10wt.%Co_xCrCuFeNi system was investigated by Chen et al. [74]. Using an equiatomic CoCrCuFeNi HEA as binder, and similarly to the results of Zhou et al. [59], the increase in sintering temperature up to 1400 °C effectively increased both Vickers hardness and fracture toughness of WC-10wt.%CoCrCuFeNi up to 1.95 GPa and 10.83 MPa·m^{1/2}, respectively, by achieving a densification of over 99 %. However, a further increase is detrimental for the mechanical properties due to the precipitation of deleterious phases and grain growth. In all these cases, the binder presented a BCC+FCC microstructure, and regardless of the sintering temperature, the densification of WC-10wt.%CoCrCuFeNi is always superior to 96 % due to the excellent wettability (0.5°) of CoCrCuFeNi over WC. In terms of the effect of Co content in the binder, the microstructure presented a major content of BCC as long as the Co content increased. Besides, a coarser grain size was observed with further Co, which was attributed to the easier diffusion of WC in the less compacted BCC phase. Although the fracture toughness values obtained with these cermets are similar to those of commercial WC-based cermets, the resultant Vickers hardness (< 2.1 GPa·m^{1/2}) are among the lowest values obtained with WC-HEAs cermet. Additionally, the effect of the C content in the microstructure of a gradient WC + CoCrCuFeNi cermet was studied by Linder et al. [73]. The authors reported that gradient microstructure is sensitive to the C content, achieving a η-phase free zone in the surface when 2.25 wt% of C was added. With an increase in C content, the composite is displaced beyond the C window, causing the disappearance of the gradient microstructure. In such instances, the resultant microstructure predominantly comprises WC, HEA binder, γ-phase, and graphite regions. Conversely, when the sample is maintained within the C window, a gradient microstructure is discernible, and there is an absence of graphite formation. These two features can be used to enhance the impact toughness of the tool by preventing crack propagation from the surface to the bulk, thereby improving the lifetime of the tool [75]. A further increase in the C content pushes the cermet equilibrium outside the C window, promoting the precipitation of free C

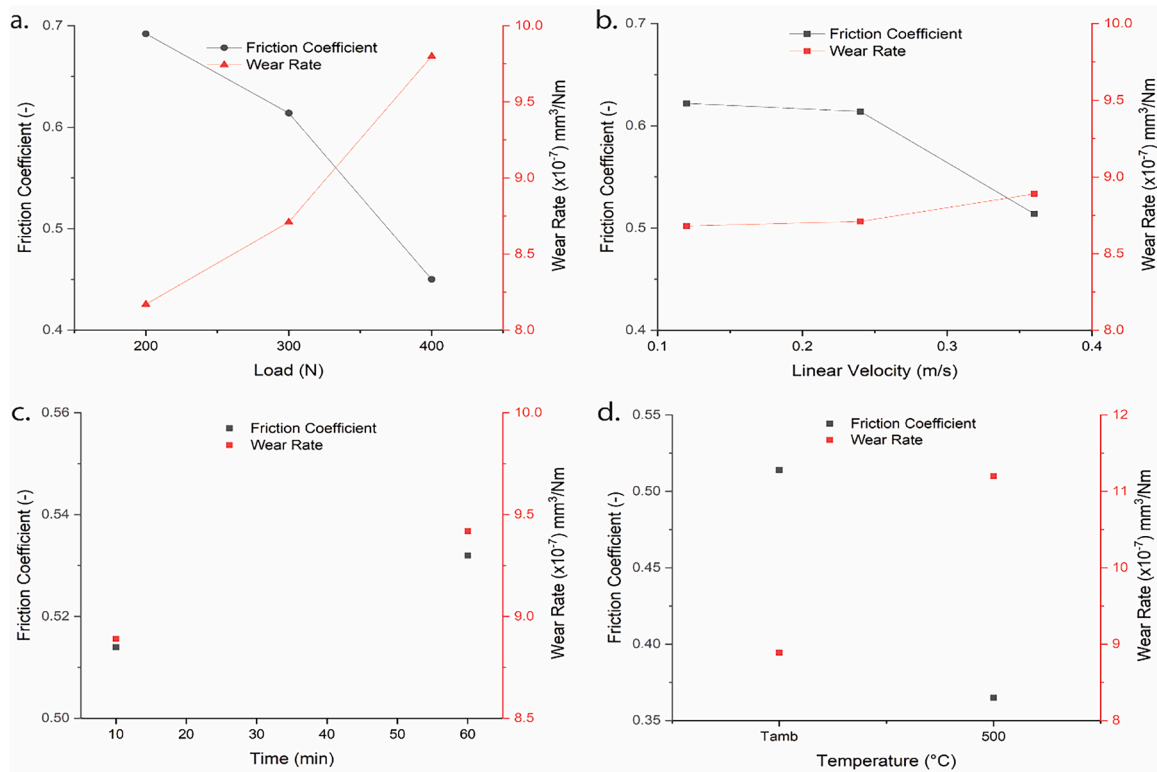


Fig. 4. Coefficient of friction (COF) and wear rate (WR) of WC-CoCrCuFeNi cermets: (a) effect of load test, (b) effect of the linear velocity at a constant load of 300 N, (c) effect of time at 300 N and $0.36 \text{ m}\cdot\text{s}^{-1}$, and (d) effect of temperature at 300 N, $0.36 \text{ m}\cdot\text{s}^{-1}$ and 10 min duration [72].

as graphite, and eliminating the gradient microstructure.

On the other hand, the processing route may have considerable effects on the microstructure and mechanical performance of WC-cermets. Unfortunately, the effect of the different fabrication variables is not straightforward and optimal conditions (that leads to the best combination of mechanical properties) must be experimentally determined. For example, Mueller-Grunts et al. [76] found that increasing the milling time from 30 min to 1h during the preparation of the WC-20wt.% CoCrCuFeNi cermet caused a raise in the Vickers hardness (from 6.78 to 10.05 GPa) in the sintered state. Nevertheless, the authors also found that a further increase up to 2h was detrimental and reduced the bulk hardness to 8.18 GPa. Hence, previous steps to the sintering stage can lead to important differences in the mechanical performance of the cermet.

At the same time, the physical and chemical features of the starting material also possess an influence on the microstructure and performance of cermets. The effect of the initial WC particle size and how Cr was introduced in the binder phase (added as Cr_3C_2 particles or doping the WC ceramic particles with Cr_3C_2 and VC nano particles) was studied by Soria-Biurrun et al. [70] employing the WC-Co-Cr-Fe-Ni system. The authors registered a 12 % reduction on the shrinkage during sintering when Cr_3C_2 and larger WC particles ($3.7 \mu\text{m}$) were used instead of smaller doped WC particles ($0.8 \mu\text{m}$), due to the lower driving force (surface area) of the larger particles and the modification of the atomical diffusivity due to the simultaneous dissolution of Cr_3C_2 and WC particles. The application of a posterior HIP process could eliminate the remaining porosity only in the samples fabricated with coarse particles, nevertheless, the best performance was attained by employing doped ultrafine WC particles, achieving 15.84 GPa, $8.1 \text{ MPa}\cdot\text{m}^{1/2}$ and 2696 MPa of Vickers hardness, fracture toughness and TRS, respectively. The resultant Vickers hardness is superior to what was reported by Soria Biurrun et al. [60] but with a slightly inferior TRS value. Nevertheless, the mechanical properties reported were lower than those obtained by Zheng et al. [71] and ultrafine grade commercial WC-Co.

2.1.4. Al-containing CoCrFeNi system

The CoCrFeNiAl HEA has been studied as binder of WC cermets too, based on their excellent mechanical properties and corrosion resistance [77–79]. Zhou et al. [59] studied the effect of the binder content and sintering temperature on the microstructure and mechanical properties of WC-CoCrFeNiAl cermet prepared using mechanical alloying, compaction and sintering. The resultant microstructure was composed by WC + FCC + η -carbides ($\text{M}_3\text{W}_3\text{C}$, $\text{M}_3\text{W}_9\text{C}_4$) + Al_2O_3 , regardless of sintering temperature or binder content. According to the authors, Al_2O_3 films around the pores are formed during the sintering process due to the Al precipitation and posterior reaction with the O_2 present in the surface of the mechanical alloyed powders. Regardless of binder content, an increase in the sintering temperature up to $1400 \text{ }^\circ\text{C}$ can effectively raise the composite hardness and compressive strength; nonetheless, further increase of the sintering temperature is detrimental for both properties. The best combination of hardness and fracture toughness reported by the authors was achieved with a 10 wt% of CoCrFeNiAl sintered at $1400 \text{ }^\circ\text{C}$ for 1h, registering 21.18 GPa and $7 \text{ MPa}\cdot\text{m}^{1/2}$, respectively.

Similarly, Chen et al. [80] studied the effect of the binder content on the mechanical properties at RT and high temperatures of the WC + CoCrFeNiAl_{0.5} cermet. The microstructure was only composed by and FCC solid solution and a WC ceramic phase, likewise to that reported by Luo et al. [81]; however, the resultant Vickers hardness (14.84 GPa) obtained by the firsts was somewhat lower to that reported by the latter (20.31 GPa). Increasing the binder content from 10 to 35 wt% straightforwardly decreased the Vickers hardness from 14.84 to 10.03 GPa and the wear resistance from $38 \text{ m}/\text{mm}^3$ to $4 \text{ m}/\text{mm}^3$. The best balance of properties was thus reported with a 20 wt% of binder, presenting a Vickers hardness of 13.86 (slightly inferior to that of WC-18wt.%Co commercial grade) and a RT fracture toughness of $17.4 \text{ MPa}\cdot\text{m}^{1/2}$ (The performance exceeds that of the commercial equivalent by 30%, marking it as the highest reported value to date). When comparing the high temperature hardness with commercial grades WC-based cermets [82], it was found that the substitution of Co by CoCrFeNiAl_{0.5} increased

the softening resistance of the composite, registering a high temperature hardness (700°C) of 7.29 GPa, almost 3GPa superior to that reported for WC-Co commercial grades at the same temperature. Contrary to the observed in [81,80], Muller-Grunts et al. [76] found that the microstructure of WC-20 wt.%CoCrFeNiAl_{0.5} was composed of the FCC solid solution and WC, but several secondary phases as W₂C, Co₃W₉C₄ and Al₂O₃ were observed too, when the C content was stoichiometric. Even more when the C content was higher, Cr₇C₃, NiAl and graphite were observed.

2.1.5. AlCu-containing CoCrFeNi system

Investigations of the CoCrCuFeNiAl HEA as binder were reported in [76,80,81,83]. Luo et al. [81] studied the effect of Al content in the WC-10wt.%CoCrCuFeNiAl_x cermet, reporting that despite the increase in the wetting angle from 0.5° to 4.6° when the Al content increases from x = 0 to x = 1.5 [84]. The cermet densification and Vickers hardness increased meanwhile the fracture toughness was not highly affected. The composites only exhibited a WC and FCC phases with a lower grain size compared to WC-Co cermets sintered under the same conditions and the best combination of mechanical properties was attained by WC-10wt.%CoCrCuFeNiAl with a 97.9 % of densification, 20.3 GPa of Vickers hardness and 10.3 MPa·m^{1/2} of fracture toughness.

One step beyond additive manufacturing, Li et al. [83] employed selective laser melting (SLM) to fabricate WC-20wt.%CoCrCuFeNiAl cermets. The sample fabricated by selective laser melting (SLM) showed a gradient microstructure along the building direction (as depicted in Fig. 5) due to the high-power laser that caused the sublimation of certain elements as well as a dilution effect due to diffusion from the substrate (made of a FeNi alloy) to the sample. In the region nearby to the

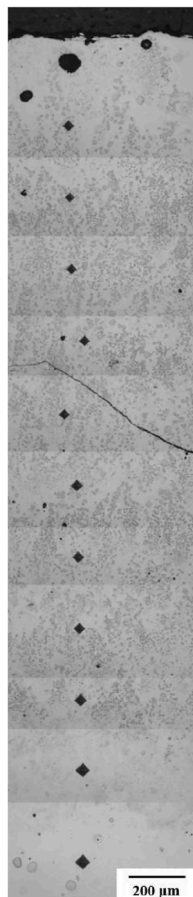


Fig. 5. Optical micrograph of the cross section of the as-built cemented carbide and the Vickers hardness impressions along the building direction [83]. Reproduced with permission of Elsevier.

substrate, the Fe, Ni and Al elements diminishes and the W, Co, Cr and Cu increases, while in the farthest region only the W element increases and the rest of element decreases. This gradient structure resulted in gradient hardness and fracture toughness, observing the highest hardness and lower toughness in the upper region and the lowest hardness and higher toughness in the lower region, attributed to the presence of dendritic W₂C (harder but more brittle than WC [85]) and the increase of carbide fraction. The properties of the upper and lower portion of the gradient composite are comparable to that of WC-12 wt.%Co and WC-25wt.%Co, respectively, however, the difficulty to control the composition of the HEA during the SLM process should be improved to synthesize a material with homogeneous microstructure and mechanical properties that could compete with cermets discussed above and/or the commercial grades.

2.1.6. Other binder compositions

On the other hand, Yadav et al. [86] investigated the effect of the binder content on the microstructure and mechanical properties of WC-Co_{27.4}Cr_{13.8}Fe_{27.4}Ni_{27.4}Mo₄ cemented carbide, proving that the cermet maintained a simple microstructure after the sintering process, being only composed by an FCC solid solution and the WC reinforcement phase. Decreasing the binder content from 20 to 10 wt% increases the Vickers hardness from 20 to 21 GPa, the compressive strength from 1.9 to 2.2 GPa, the Weibull modulus from 7.98 to 9.72 and contrary to that reported the previous authors, the fracture toughness also increases from 9.43 to 10.5 MPa·m^{1/2}. Incorporating Mo in the composition of the binder phase suppress the formation of Cr₇C₃ carbide during the sintering process, inhibit grain growth and increases the hardness by solid solution, which enhances the TRS, corrosion and abrasion resistance of the alloy. The results obtained with this binder are superior to those obtained by Zou et al. (19.5 GPa and 10.96 MPa·m^{1/2}) [58], Lou et al. (19.47 GPa and 10.15 MPa·m^{1/2}) [87] and even commercial grades [88,89]. This suggest that this high-entropy alloy could exhibit a very interesting performance as binder of cermets for metal cutting, rock and mining industries.

Zhou et al. [56] studied the effect of the binder content on the microstructure and mechanical properties of WC-CoCrFeNiTiAl cermet, obtaining a microstructure composed only by a BCC solid solution and a WC ceramic phase. Contrary to that observed by the previous authors, an increase in the binder content from 10 to 20 wt% increases the fracture toughness, the Vickers hardness, and the compression strength from 8.33 MPa·m^{1/2}, 21.88 GPa and 5219 MPa to 12.1 MPa·m^{1/2}, 23.12 GPa and 5420 MPa, respectively. As could be seen, the best performance was attained by using 10 wt% of HEA as sintering aid and while the hardness and toughness is somewhat similar to the WC-10 wt.%CoCrFeNi cermet fabricated by Zheng et al. [71] (18.95 GPa and 15.88 MPa·m^{1/2}), the TRS value is the highest reported until now, making this cermet a very good candidate to replace the commercial WC-based cermets.

The effect of binder content and aging temperature in the Vickers hardness and microstructure of WC-CoCrTiNiAl cermets was studied by Biurun et al. [90]. Regardless of the binder content, the cermet was constituted by WC, FCC solid solution, and *in situ* formed (Ti_{0.8}W_{0.2})C carbides and Ni₃Al precipitates. As the metallic content increased from 14.2 to 30.4 wt%, the as HIP-ed Vickers hardness only decreased from 12.21 to 11.49 GPa. Regarding the aging treatment, it was found that the maximum binder hardness is obtained at lower aging temperatures as the Al content increases. This results from the higher driving force for precipitation as the Al supersaturation is greater after the solution treatment. However, despite to the aging effect observed in previous reports [60], the aging treatment slightly reduces the Vickers hardness and TRS values of the as HIP-ed cermet from 8.99 GPa and 2423 MPa to 8.88 GPa and 2376 MPa, though, the hardness of the binder increases from 11.8 GPa to 13.9 GPa, showing a hardening effect due to gamma prime precipitation. The previous reveals that the aging treatment could be a good strategy to improve the mechanical properties, although

detailed further studies are required to effectively control the aging process and achieve a better combination of mechanical properties.

In a second study, the authors investigated the effect of milling time, metallic content and aging time at 600 °C with different additions of AlN or TiAl₃ in the microstructure and performance of WC-CoCrTiNiAl cermets [91]. They reported that a better alloying effect, in terms of dissolution of compounds in the metallic matrix, was obtained when aluminum is incorporated in form of Ti₃Al instead of AlN due to its higher dissolution rate during the liquid phase sintering. A finer microstructure is obtained when more Al is dissolved in the binder phase during sintering, observing a lower WC grain size when the Al is incorporated in for of Ti₃Al (1.2 μm) instead of AlN (2.1 μm). Results that are in concordance with prior investigations substantiate the assertion regarding the efficacy of Al as a proficient inhibitor of WC grain growth during the sintering process and the improvement on the thermal stability [92]. As the milling time or the Al content in the binder increases, the WC grain growth is diminished due to the precipitation of γ and the presence of Al itself [92].

Nakonechnyi et al. [93] studied the effect of the sintering temperature and time in the performance of the WC-10 wt.%CrFeNiMoW cemented carbide employing electron beam sintering technique. Regardless the sintering temperature or time, the microstructure was composed by an BCC solid solution, WC reinforcement phase and (Cr, Fe, Ni)_xW_yC_z complex carbide, associated with the presence of a thin oxide layer on WC and HEA particles and to the process of C depletion of WC [94]. Additionally, the consolidation of the EBS-ed cermets was improved by both, the sintering temperature and the sintering time, an increase in the relative density from 70.07 to 98.8 % was observed when the temperature increased from 1250 °C to 1450 °C while maintaining 4 min of sintering time. Similar results are obtained if the sintering temperature was kept at 1450 °C and the sintering time increased from 10 s to 4 min, registering an increase in densification from 73.5 to 98.8 %. The best combination of hardness and toughness was obtained using a sintering temperature of 1450 °C for 4 min, achieving a WC grain size between 1 and 5 μm, a binder grain size between 0.3 and 0.5 μm, 18.9 GPa of hardness and a fracture toughness of 11.4 MPa·m^{1/2}.

2.2. TiC- and Ti(C,N)-HEAs cermets

Ti(C,N)-based cermets are characterized by adequate high-temperature hardness, good chemical stability, superior ductility, and higher wear and oxidation resistances that WC traditional cermet [95–98]. The properties of the Ti(C,N) are directly related to the basic characteristics of TiC and TiN, since these two are the basis for the Ti(C,N) [96]. All of them exhibit a fcc lattice structure, where both C and N atoms share (with complete solubility) the octahedral interstitial sites of the lattice formed by Ti atoms (see Fig. 6) [99]. Table 1 summarizes some of the physical and mechanical properties of the TiC, TiN and different composition of C and N in the Ti(C,N).

The development of the Ti(C,N)-based cermets began with the improvement of the wettability of the binder in the TiC-Ni cermet. In the

first instance, the addition of Mo allowed complete wetting of TiC with the binder, promoted a more uniformly dispersed TiC structure which improved its mechanical properties, due to refinement of carbide grain size, but there is a strong tendency for Mo to diffuse into carbide phase [102,103]. These cermets show a characteristic rim-core structure, where the core remains with the composition of the original ceramic, and the rim corresponds to a (Ti,Mo)C [104]. This feature allows various metals to dissolve and re-precipitate in the carbide or carbonitride phase during the sintering stage, developing complex rim solid solutions of (Ti, M)(C,N), where M can be W, Mo, Ta, among others. This microstructural feature can be obtained by adding these elements in the binder, or by using secondary carbides (such as Mo₂C, VC, WC, NbC, among others) [95,96,99,101,104–108]. A simplified schematic of the powder blending and microstructure of the Ti(C,N)-based cermet with secondary carbides is presented in Fig. 7a and b, respectively. In this latter, the hard phases consist of a core of carbides or carbonitrides surrounded by one or two rings with complex composition, embedded in the metallic matrix (this last represented in yellow). In the image, the black core consists of TiC/Ti(C,N), white phase is a carbide or carbonitride rich in heavy metals (Ta, Mo, V, W, Nb, among others), and the gray phases is the closest thing to the equilibrium composition of the hard phase formed when the secondary carbides dissolve in the structure of TiC or Ti(C,N). This last is usually referred as a coreless grain. Fig. 7c schematizes the composition profile of a core-rim hard phase grain and the surrounding binder phase. In this, it can be observed that the core contains the highest amount of TiC/Ti(C,N), surrounded by the inner ring, with high presence of the secondary carbide components added in the cermet, and by the outer ring with a distribution similar to the equilibrium composition of the hard phase.

The addition of TiN or N, in a particular study, increases the amount of binder in the cermet whatever the initial Ni percentage, improving fracture toughness, as well as preventing Mo diffusion [101,104]. The effect in the microstructure and mechanical properties are summarized in Table 2, where the presence of N leads to a drop of Young's modulus, hardness and density value. For the cermets with 25 wt% of Ni as binder, the grains and rims size are smaller with the addition of TiN, where it acts as a grain growth inhibitor [104]. Nevertheless, this effect is not present in the other composites (higher TiC content in the mixture), where the amount of rim and core phase volumetric increases, manifesting a higher decomposition of TiC or TiCN [101]. Then, the effect of inhibiting grain growth and hard phase decomposition by adding N to the system depends on the C/N ratio in Ti(CN)-based cermet, more than binder content.

Despite the excellent characteristics of Ti(C,N)-based cermets, these exhibit lesser mechanical properties than WC-based cermets. Continuous efforts to improve the toughness of TiC-based cermets have led to employ HEAs as binder in Ti(C,N) cermets, aiming for a good balance between mechanical strength and toughness, characteristics that can be further improved by adding different elements that can affect the hard phase. These elements not only improve the strength and toughness of the hard phase but also enhance the wettability of the hard particles with the binder phase during liquid phase sintering [99], reducing the coalescence of the particles and promoting a more uniformly dispersed ceramic structure [102].

Table S2 (Supplementary Material) summarizes the fabrication method, the microstructural features, and mechanical properties of Ti(C,N)-HEAs cermets. As can be appreciated, these comprises complex hard phase compositions, obtained by the mixture of several carbides during the blending and milling stage therefore. On the other hand, as just as with the WC-HEAs cermets, FCC-stabilizing elements are commonly occupied in the binder composition, conducting to mostly FCC binder microstructures. An exception of this was the cermet reported by Liu et al. [110], who mixed WC, Mo₂C, TaC, NbC and VC powders with Ti elemental powders and employed reactive synthesis for the obtention of the cermet. Hence, the bulk cermet exhibited Ti-rich carbides partially enriched with Nb and Ta, bonded by a MoVWNbTa BCC phase – a

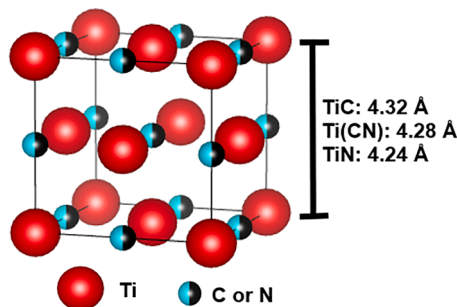


Fig. 6. Illustration of the lattice structure of TiC, TiN or Ti(CN).

Table 1
Physical and mechanical properties of TiC, TiN, and Ti(C_xN_{1-x}) (with x = 0.3, 0.5, 0.7) [99–101].

Hard Particle	Lattice Parameter (Å)	Hardness(GPa)	K _{Ic} (MPa·m ^{1/2})	σ _{ys} (MPa)	E (GPa)	k (600 °C aprox.)(W/m ² /°C)	σ (μ-Ω·cm)
TiC	4.320	31.38	–	–	–	16	–
TiC _{0.7} N _{0.3}	4.296	20.79	5.7	330	510	17.5	95.1
TiC _{0.5} N _{0.5}	4.280	20.59	6.3	435	473	22.5	76.6
TiC _{0.3} N _{0.7}	4.265	17.06	5.4	360	467	25	52.3
TiN	4.240	19.61	–	–	–	28	–

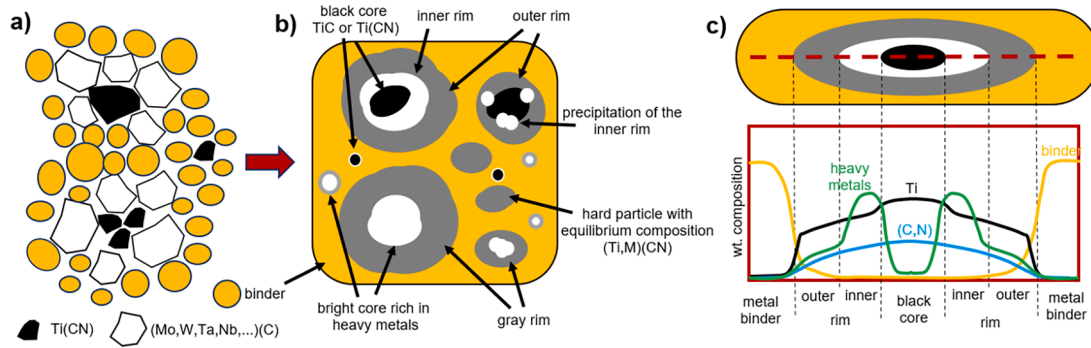


Fig. 7. Schematic of the morphology of the possible microstructure of the Ti(CN) based cermet with secondary carbides: a) powder distribution in the green sample (before sintering process), b) microstructure of cermet, with the different structures on the cermet, such as, black core-gray rim, inner and outer rim, bright core-gray rim, bright and black particles, and solid solution hard particles (phase in equilibrium composition respect to the hard particles), c) hypothetical composition profile of a hard particle with black core-inner and outer rim [101,104,107–109].

Table 2

Average grain size, volume proportions of rims, cores, and binder, and mechanical properties of cermet's TiC-TiN-Mo₂C-Ni [101,104].

Cermet	xTiC-yTiN-10Mo ₂ C-25Ni		xTiC-yTiN-10Mo ₂ C-20Ni		xTiC-yTiN-10Mo ₂ C-15Ni	
	x = 65; y = 0	x = 55; y = 10	x = 70; y = 0	x = 60; y = 10	x = 75; y = 0	x = 65; y = 10
Grain size (μm)	4.2	2.4	2.3	3.2	2.8	3.6
Binder (%)	10.1	21.4	11.2	13	8.7	10
Core (%)	6.5	6.7	30.4	18	26.8	11
Rim (%)	83.4	71.9	58.4	69	64.5	79
Density (g/cm ³)	5.32	5.15	5.58	5.56	5.42	5.41
E (GPa)	370	290	400	390	410	396
H _v (GPa)	1510	1270	1360	1235	1520	1420
K _{Ic} (MPa·m ^{1/2})	6.0	10.0	13.8	14.2	10.3	13.6

refractory high-entropy alloy (RHEA) binder [111]. The TiC-RHEA composite exhibited a RT compressive strength of 3060 MPa and a fracture surface corresponding to brittle transgranular cracks and quasi-cleavage fracture. The high strength was attributed to the solid solution strengthening mechanism, both in the binder and in the carbide.

Returning to 3d TM HEAs binders, research has shown that among typical HEAs constituent elements, Cr has the strongest interaction with the ceramic phase. For example, Rogachev et al. [112,113] reported rounded TiC grains with a dissolution of up to 1 wt% of Cr on them, using three different HEAs as binders: CoFeNiCrMn, CoFeNiCrTi and CoFeNiCrAl. According to the authors, the presence of Ti in the binder resulted in a slightly larger TiC grain size, while the addition of Al resulted in the highest hardness (17.7 GPa) as well as the highest BCC/FCC phase fraction ratio. On the other hand, De la Opra et al. [114] evaluated the effect of different constituent elements on the stability of Ti(C,N)-based cermets. Four different HEAs were used for this purpose: CoFeNiCrCu, CoFeNiCrMn, CoFeNiCrV, and CoFeNiMnV; where Cr-

containing alloys exhibited Ti-Cr-rich regions in both vicinities of the ceramic-binder interface, while dissolution of Ti into the binder was observed in all the cases. Cu addition produced the precipitation of a secondary Cu-rich FCC phase, meanwhile a loss of up to 14 % of Mn was observed in the CoFeNiCrMn binder, attributed to Mn sublimation. V-containing cermets presented a core-rim structure, due to the dissolution of V into the carbonitride grains.

Years before, De la Opra et al. [115] had synthesized a (Ti_{0.8}Ti_{0.1}Nb_{0.1})(C,N)-based cermets employing CoFeNiCrMn and CoFeNiCrV as binders (both HEAs possessed only a FCC phase in the powder state). While the CoFeNiCrMn was constituted by a FCC solid solution and C14 Laves phase, the CoFeNiCrV binder suffered a complete transformation only presenting sigma and C14 Laves phases. According to the authors, the formation of these intermetallic compounds was induced for the excessive dissolution of the ceramic particles in the molten alloy during sintering, saturating the binder in Ti, Nb and Ta, promoted by using a non-stoichiometric carbonitride phase (Ti_{0.8}Ti_{0.1}Nb_{0.1})(C_{0.5}N_{0.3}). When an additional 1.8 wt% of graphite was incorporated in the initial mixture, the amount of Ti, Ta and Nb in the binder phase was reduced, the carbonitride dissolution was hindered, and a fully-FCC microstructure of the binder in the CoFeNiCrV-based cermet was observed. Although the addition of graphite resulted in an enhanced toughness, the hardness was severely affected: even more, these cermets have the worst combination of hardness and toughness of those presented in this section (see Table S2). The researchers determined that these results were caused by poor densification, due to the low wettability of the binder.

The presence of C14 Laves phase and (Ti,Ta,Nb)C_{1-x} Hägg phase were reported in the investigation of Real et al. [116], synthesizing Ti(C,N)-20vol.%CoFeNiCrMnAl_x (x = 0, 0.3, 0.5) cermets obtained by reactive sintering, employing (Ti_{0.8}Ta_{0.1}Nb_{0.1})(C,N) as ceramic phase. In addition, the microstructure of the sintered cermet showed (Ti,Ta,Nb)(C,N) complex carbonitride and FCC solid solution. The research was focused on the mean free path (related to densification) and the coarsening rate constant, where both increases with the increase of sintering temperature and Al content. At the same time, the sample with no Al

exhibited the highest activation energy (236.1 kJ/mol) conducting to the smaller particle size (2.95 μm) and the highest hardness (12.6 GPa) among the studied samples. Better results were presented by Lin et al. [117], synthesizing to TiC-based cermet using $\text{Co}_{1.5}\text{CrFeNi}_{1.5}\text{Ti}_{0.5}$ as binder, comparing it with Ni and $\text{Ni}_{13}\text{Mo}_7$, produced by LPS. A superior wettability and activation energy (788.8 kJ/mol) was found in the TiC-HEA cermet in comparison to traditional ones, since a thin layer of Fe, Co, and Ni was formed around the carbide grains. The use of the HEA as the binder did not result in a core-rim structure, like in the TiC- $\text{Ni}_{13}\text{Mo}_7$, but small amounts of Cr were dissolved in the carbide. Hence, the TiC-HEA presented the highest hardness and smallest grain size between the three cermets (18.4 GPa and 0.435 μm), but a lower fracture toughness than TiC-Ni. The grain size reported corresponds to the smallest one among the cermets presented in the current section.

Fig. 8 shows a plot of hardness vs sintering temperature of Ti(C,N)-based cermet of three studies.; Ti(C,N)-20vol.%CoFeNiCrMnAl_x (x = 0, 0.3, 0.5) [116] referred to above; cermet contain 25 wt% TiB₂ as a secondary ceramic and CoFeNiCrAl as binder phase [118], this study will be presented later; and Ti(C,N)-CoCrNiCuMn cermet, using powders of TiN_{0.3} and TiC in a wt. ratio of 72:28 [119]. In this last, the cermet with 7 wt% of binder was sintered at different temperatures, where the best performance was obtained at 1400 °C, with hardness and toughness values of 17 GPa and 6 – 7 MPa·m^{1/2}, respectively, since it is the condition with the best results. This composite differs from the others by having less coarse grains with presence of *trans*-granular fracture. Despite of that cermet sintered at 1450 °C does not show *trans*-granular fracture, its lower hardness is a consequence of higher grain growth. The main fracture mechanism is inter-granular fracture, in all hard composites. In Cermets with variation in Al content, the microhardness decreased with the rising of sintering temperature, favored the phase segregation and the formation of intermetallic compounds which brittleness the cermet [116]. The reduction in particle size acts as the main strengthening mechanism in these composites. In the case of Li et al. [120] study, the behavior of hardness is related to poor wettability and grain growth at low (1450 °C) and high (1650 °C) sintering temperature. The result of fracture toughness is closely related to the wettability of CoFeNiCrAl with the Ti(C,N) and TiB₂, where the molten HEA almost completely spreads onto the Ti(C,N), with a contact angle of 5.3°.

The tribological properties of Ti(C,N)-HEAs cermets have been studied too, as can be appreciated from Table 3; this summarizes the tribological tests and results published up to the date of this article. Wang et al. [121] studied the tribological performance of Ti(C,N)-15wt.%CoCrFeNiCu cermets employing a mixture of Ti(C_{0.7}N_{0.3}), WC, Mo₂C,

and TaC for the ceramic phase, and either gas-atomized HEA powder (a1HEA), MA-ed powder (mHEA) and Ni. Compared to the cermet with conventional binder, both HEA-cermets showed less growth of core-rim structures and promoted the formation of coreless-grains (complete solid solution of hard phase). More intergranular fracture is shown in crack propagation paths of both HEA-based cermet, with presence of transgranular fracture, crack deflection and grain pull-out, compared to traditional Ni as binder. The Ti(C,N)-maHEA condition and Ni binder present a Laves phases with a hexagonal structure similar to Fe₂W and Ni₃Ti, respectively. Besides, results of tribological testing at 600 and 800 °C (dry sliding ball on disk at 1000 rpm and 10N) resulted in a superior lubrication performance and wear resistance of HEA-based cermets. These exhibited the formation and delamination of a tribo-oxide layer; meanwhile, Ti(C,N)-Ni cermet additionally exhibited abrasive wear due to debris and particle detachment.

Similar study was realized for Chai et al. [122] synthesizing two Ti (C_{0.7}N_{0.3})-10wt.%Mo₂C-15wt.%CoCrFeMnNi cermet, using either gas-atomized HEA powders (a2HEA), a mixture of pure elemental powders of Co, Cr, Fe, Mn, (mxHEA), and Ni as binders. In HEA-cermet cases, the ceramic phase exhibited a typical core-rim structure (attributed to the dissolution of the Mo carbide) and coreless grains, meanwhile the binder presented a Ti,Mo-rich FCC phase and intermetallic C14 Laves phase similar to Fe₂Ti, with no effect on densification. While intergranular fracture was the main mode of fracture in the cermets, the Ti(C,N)-a2HEA exhibited crack deflections, grain pull-out, bridging, and crack branching that improved the hardness. Both studies showed the less grain size with the gas atomized HEA condition, 0.87 and 1.05 μm for a1HEA and a2HEA, respectively, this last one had a relative density 99.32 %. The authors also reported the characteristics of Ti(C,N)-HEA cermet used as substrates for the Chemical Vapor Deposition (CVD) of a multilayer coating of TiN/Al₂O₃/TiCN. A summary of the quality of the deposited coating is presented in Table 4. The coating using the Ti(C, N)-a2HEA as a substrate exhibited the best resistance to adhesion failure – classified as HF1 – and a lower wear rate compared to that using Ti(C, N)-Ni substrate, although this last one exhibited a lower friction coefficient fluctuation and shorter time in the transition stage. A best wear resistance was obtained in the HEA-cermets, due to the presence of flakes and complete oxide aluminum layers on the worn surface, in the mxHEA and a2HEA cases, respectively. The COF fluctuated 0.45–0.6 for both HEA-containing cermets (indicated in the Table 3), and the lower wear rate while the lower wear rate was obtained in the a2HEA-containing cermet.

On the other hand, Liu et al. [127] deposited a multi-layer nano CrAlN/TiAlN coating in to a synthesized Ti(C,N)-based cermets with three different atomized HEAs powder – CrFeCoNiMo, CrFeCoNiMn and CrFeCoNiAl – as binders, whose mechanical properties are presented in Table 5. The cermets showed a typical “core-rim” structure with two FCC structures, corresponding to Ti(C,N) and a high-entropy solid solution phase (see Fig. 9). Using CrFeCoNiAl as binder resulted in the multi-layer coating deposited on the cermet with the highest densification and mechanical properties, exhibiting a dense and smooth surface with few micro voids and particles. A similar coating morphology was obtained in the case of cermets with Ni/Co binder, but the smaller grain size of the substrate Ti(C,N)-CrFeCoNiAl allowed to obtain a more dense and thinner coating. On the contrary, the microstructure of the coatings on the other two cermets, showed rough morphology and irregular surface with a few pores. A greater volume of binder phase in the microstructure of these cermets, worsened the deposition of the coating since the nucleation of the coating preferentially developed in the Ti(CN) phase. Comparing these two cermets, the Mo-content exhibited a finer average grain size, which provided more nucleation points for the coating growth. It attributed a little denser and thinner coating on cermets and has better properties that the cermet with Mn-content.

Yang et al. [123] studied the effect of progressively replacing Ni with CrMnFeCoNi on the mechanical and tribological properties of Ti(C,N)-

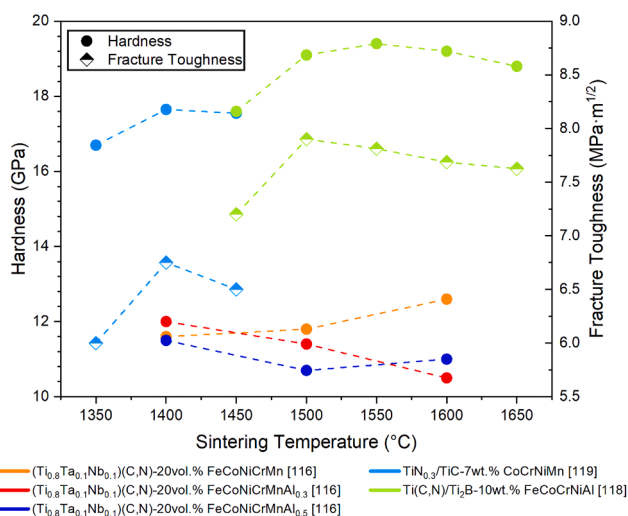


Fig. 8. Hardness vs Sintering temperature of Ti(C,N)-based cermets [116,119,120].

Table 3
Tribological characterization performed on HEA Ti(C,N)-based cermets.

Composition	Counterbody	Test Condition	COF	Wear rate (mm ³ ·N ⁻¹ ·m ⁻¹)	Ref
Ti(C,N) – WC – Mo ₂ C – TaC15 wt. % CoCrFeNiCu	Steel Cemented carbideGCr15 Steel ball	Dry sliding (ball on disk)1000 rpm, 10 N, 600 °C/800 °C	600 °C: 0.34–0.38800 °C: 0.21–0.25	600 °C: 7.5–10 × 10 ⁻⁶ 800 °C: 8.5–12.5 × 10 ⁻⁶	[121]
Ti(C,N) – Mo ₂ C 15 wt% CoCrFeMnNi CVD Coating (TiN/Al ₂ O ₃ /TiCN)	ASTM51200 steel	Dry sliding (ball and disk)2000 rpm, 5 N, 700 °C,30 min	0.45–0.6	3–3.5 × 10 ⁻⁹	[122]
Ti(C,N) – WC – Mo ₂ C – TaC 15 wt% Ni/CrMnFeCoNi	Si ₃ N ₄	Dry sliding (ball on disk)1000 rpm, 10 N, 750 °C	0.48–0.75	15.16–8.82 × 10 ⁻⁶	[123]
Ti(C,N) – WC – Mo ₂ C – TaC 10 wt% Al _{0.3} CoCrFeNi	Steel cemented carbide	Dry sliding (pin on disk)200 rpm, 4.9 N, 900 °C, 10 min	0.13	–	[124]
Ti(C,N) – WC – Mo ₂ C – xNbC15 wt. % CoCrFeNi	Steel cemented carbideGCr15 Steel ball	Dry sliding (ball on disk)1000 rpm, 10 N, 700 °C	0.284–0.198	4.14–14.7 × 10 ⁻⁶	[125]
Ti(C,N) – TiB ₂ 10 wt. % FeCoCrNiAl	Cemented carbideWC-6Co	Dry sliding 450 rpm, 5 N, 200–800 °C, 20 min	0.23–0.36	9.8–1.7 × 10 ⁻⁵	[126]

Table 4
Properties of the coatings TiN/Al₂O₃/TiCN on the Ti(C,N)-based cermets as substrate [122].

Grain size of Coating	Binder of SubstrateTi(C,N)	Critical Loads Lc (N)	Hardness (GPa)	Coating classified
TiN/ Al ₂ O ₃ / TiCN(nm)	-Mo ₂ C-15wt.%binder			
22.1/34.2/ 15.0	CoCrFeMnNi (atomized HEA powder condition)	123	23.61	HF1
22.9/36.4/ 16.2	CoCrFeMnNi (elemental powders HEA condition)	115	26.4	HF2
23.3/37.6/ 25.9	Ni	91	23.61	HF3

based cermets. The (15 wt%-x)Ni-xHEA binder (with x = 0, 5, 10, 15 wt %) was blended with 60wt.%Ti(C_{0.7}N_{0.3}), 19wt.%WC, 4wt.%Mo₂C, and 2wt.%TaC and sintered at 1310 °C. Table 6 summarizes the properties of the resultant cermet, together with those obtained by sliding wear tests to 750 °C and dry cutting test. With the increment of HEA content, the relative density decreased, affected by the lower wettability of HEA with the hard phase, gas stored in its structure, pores of gas-atomized HEA powders, and Mn sublimation. The worst tribological response was obtained with the traditional binder (not containing HEA), but the only addition of 5 wt% of HEA on the binder, significantly improved fracture toughness, COF and wear rate. Additionally, this last sample also presented the minimum wear depth and cross-sectional area of the worn scar. Furthermore, the cermet with a fully-HEA binder presented the best cutting time, however, with almost the same wear resistance that the fully-traditional binder.

The highest fracture toughness among Ti(C,N)-HEAs cermets (11.5 MPa·m^{1/2}) was reported by Zhu et al. [128,129]. This cermet was obtained by blending different carbides (Ti(C_{0.7}N_{0.3}), WC, Mo₂C and TaC) with a 15 wt% of MA-ed AlCoCrFeNi powders, followed by sintering at 1500 °C for 1h. The cermet presented a core-rim structure, as depicted in Fig. 10, with a high Cr content in the rim phase, as well as coreless

Table 5
Properties of the coating CrAlN/TiAlN on the Ti(C,N)-based cermet as substrate [127].

Thickness of coating CrAlN/TiAlN (μm)	Binder of substrateTi(C,N) – TaC – Mo ₂ C – WC – 18 wt% binder	Mismatch degree (%)		Critical Loads (N)	Nano Hardness(GPa)	Elastic modulus(GPa)
		CrAlN substrate	CrAlN TiAlN			
1.67	CrFeCoNiMo	3.477	3.05	46.36	29.4	414
2.63	CrFeCoNiMn	3.480	3.23	43.89	28.5	411
1.10	CrFeCoNiAl	3.458	3.16	68.11	33.5	445
1.25	Ni/Co	3.460	3.32	56.18	31.3	426

grains. The binder presented two fcc phases with different amounts of dissolved W (position 3 and 4 in Fig. 10(a)), where the volume fraction of the W-rich phase is predominant. For these cermets, the improvement in fracture toughness is attributed to the higher presence of coreless grains, unlike the cermet with Ni/Co as binder (see Fig. 10 (c)), with a K_{IC} of 9.21 MPa·m^{1/2}. The authors inferred that the interfacial areas of the core/rim interface could be potential crack-initiation sites. A similar binder was employed in the work of Fang et al. [124], where the 40wt.%Ti(C,N) – 10wt.%WC – 5wt.%Mo₂C – 5wt.%TaC – 10wt.%Al_{0.3}CoCrFeNi cermet presented the highest RT microhardness reported in this section (20.1 GPa) as well as an elevated hardness of 11.2 GPa at 1000 °C. The research reports an improvement on the mechanical properties at RT and 1000 °C of this cermet when compared with the Ni/Co bonded cermet. Only the flexural strength was 1.54–1.08 times less than that that was obtained for the cermet with traditional binder, with 1488–826 MPa at RM and 1000 °C, respectively. Finally, the COF and the groove widths obtained with the 900 °C wear tests were 0.13 and 49 μm, better than the cermet with conventional binder (whose COF and grooves width was 0.21 and 172 μm, respectively).

Gou et al. [125] study the influence of NbC additions (0, 3, 6, and 9 wt pct.) on Ti(C,N)-15wt.%CoCrFeNi cermet. Although a typical core-rim structure was observed in all the cases, the increase of NbC fraction promoted grain growth and a higher proportion of coreless hard-phase grains (Ti,Nb,W,Mo)(C,N). Additionally, it also caused less dissolution of refractory metals in the binder phase. The addition of 3 wt % of NbC resulted in the highest mechanical resistance and tribological performance in a cutting and high temperature sliding wear test, presenting COF and wear rate values of 0.198 and 4.14 × 10⁻⁶ mm³·N⁻¹·m⁻¹, respectively. Higher NbC proportions worsened the cutting performance and fracture toughness, promoting transgranular crack propagation. Fig. 11 illustrates the apparition of cracks and tip breakage in the cermet inserts. The adhesive wear mechanism is dominant, where the tribolayer contains a presence of Fe, O, and a trace of hard phase elements of Ti, W, Mo and Nb.

Li et al. [118] studied the effect of the addition of TiB₂ as a secondary reinforcement particle in Ti(C,N)-Xwt.%TiB₂-10wt.%FeCoCrNiAl cermet (with X = 0, 11.5, 15.0, 22.5, 45). The cermets presented a BCC

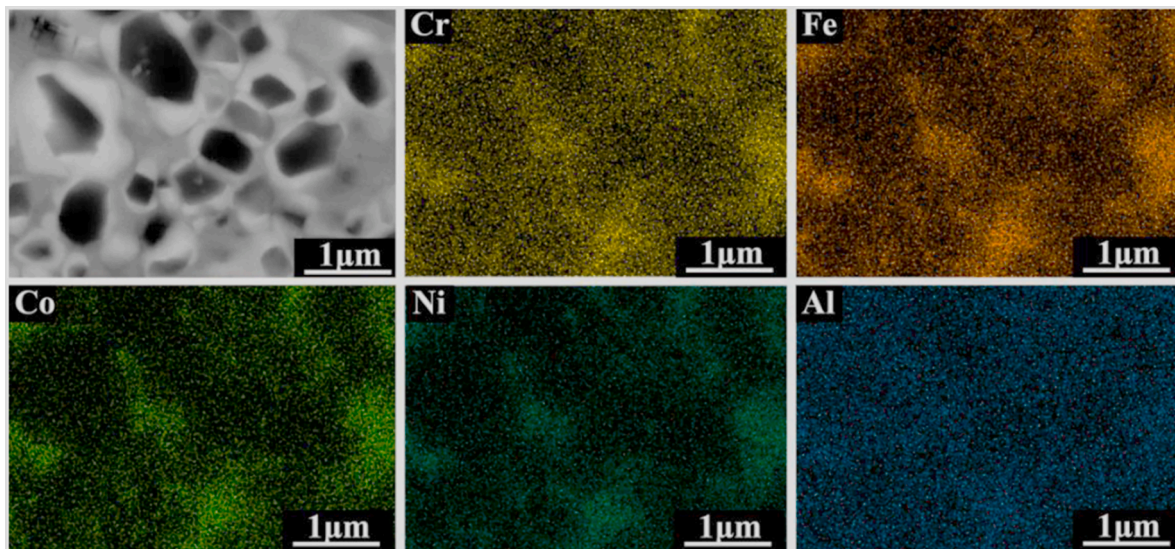


Fig. 9. EDS maps of Ti(C,N)-based cermet with 18wt.%CrFeCoNiAl as binder [127]. Reproduced with permission of Elsevier.

Table 6

Physical, mechanical, and tribological properties of Ni-CrMnFeCoNi cermets [123].

Binder	Grain size (μm)	Relative density (%)	TRS (MPa)	Hardness(GPa)	K_{IC} ($\text{MPa}\cdot\text{m}^{1/2}$)	COF(-)	Wear rate ($\text{mm}^3\cdot\text{N}^{-1}\cdot\text{m}^{-1}$)	Cutting time(min)
15 wt% Ni	0.90	99.17	2181	14.39	8.5	0.75	15.16×10^{-6}	28
10 wt% Ni + 5 wt% HEA	0.83	99.00	1757	16.17	9.1	0.48	8.82×10^{-6}	36
5 wt% Ni + 10 wt% HEA	0.80	98.75	1790	17.15	8.3	0.56	11.65×10^{-6}	37
15 wt% HEA	0.75	98.37	1490	16.86	8.1	0.65	14.85×10^{-6}	47

phase as a binder, and TiB_2 and Ti(C,N) grains. With the increment of TiB_2 content, the grain size reduced from 3.6 to 1.5 μm , while the microhardness incremented from 17.9 to 19.7 GPa. Although, the bending strength and fracture toughness was maximum with 22.5 wt% of TiB_2 with a density relative of 98.86 %. The addition of TiB_2 worsened the densification process of composite cermets, decreasing the relative density from 99.20 to 95.54 %. In a previous article [120], the group studied the effect of sintering temperature over mechanical properties, (see Fig. 8), finding that the cermet with 22.5 wt% of TiB_2 presented different crack propagation modes: transgranular and intergranular in the vicinity of Ti(C,N) grains, and grain fracture in the vicinities of TiB_2 grains. Besides of that, the cermet presented a superior hardness at 1000 °C that traditional Ni/Co-based cermet (see Fig. 12).

A complementary study was realized by Li et al. [126] employing 6, 10 and 14 wt% of HEA as binder for the Ti(C,N)- TiB_2 -FeCoCrNiAl cermet. A Ti(C,N): TiB_2 mass ratio of 3:1 was used for the ceramic phase. Hardness, fracture toughness and bending strength values of 18.6–19.3–19.7 GPa, 7.26–7.90–7.73 $\text{MPa}\cdot\text{m}^{1/2}$ and 652–727 – 720 MPa, were obtained, respectively. The tribological properties tested in vacuum were carried out at 200 – 800 °C for the 10 wt% of HEA and Ni/Co as binder, with a counter body of WC-6wt.%Co, then the COFs and wear rates of traditional binder was highest. The WR of the two materials reduced almost 5 times with increased of test temperature. At 200 and 400 °C the wear rate were $8 - 9 \times 10^{-5} \text{ mm}^3\cdot\text{N}^{-1}\cdot\text{m}^{-1}$, respectively, to cermet with HEA as binder, where the wear mechanism is mainly abrasive wear. The inferior COF and wear rate was obtained at 800°C with 0.23 and $1.7 \times 10^{-5} \text{ mm}^3\cdot\text{N}^{-1}\cdot\text{m}^{-1}$, respectively. The wear scar surface has a shallow and flat plow marks, with a relatively smooth wear surface versus 600 °C. In this case, the tribo-oxidative wear is the main wear mechanism, while the Ni/Co cermet presented adhesive and abrasive wear. A comparative high temperature hardness with the counter body (WC-6wt.%Co) indicated that cermet with 10 wt% of HEA as binder has an excellent high temperature softening resistance

compared to WC-based cermet, because its hardness is 14.51 and 13.04 GPa at 600 °C and 800 °C, respectively, 1.05 and 1.33 times higher that counter body.

The enhanced properties obtained in cermets with HEA as binder rather than with Ni/Co can be attributed to the differences in grain size and hardness, with a slight improvement in fracture toughness. Summarizing, the microstructure of HEA-containing cermets presents the typical core-rim structure of traditional Ti(C,N)-based cermets, although with a finer grain size, smaller size of the rim region, and a greater amount of coreless grains. This is a direct consequence of the low solubility of the hard particles components in the multicomponent binder, as well as the lower grain growth kinetics, promoted by the complex composition of HEAs. It should be noted that the most studied binder corresponds to CoCrFeNi containing different amounts of Al, which stand out for their fracture toughness, a property that depends on the intrinsic characteristics of the binder and its interaction with the hard phases. Regarding the tribological properties reported, cermets with HEA as binder have outperformed those with traditional binder in all aspects, despite presenting poorer densification, TRS and/or K_{IC} .

2.3. TiB_2 -HEAs cermets

Titanium diboride (TiB_2) is a good candidate to be considered as a potential hard phase due to its attractive mechanical properties – similar to those of WC – like extraordinarily high hardness (25 – 35 GPa) that could be retained up to high temperatures, high elastic modulus and flexural strength (560 GPa and >500 MPa respectively) and good thermal conductivity (60 – 120 $\text{W}\cdot\text{m}^{-1}\cdot\text{K}^{-1}$). Additionally, it presents higher electrical conductivity ($10^6 \text{ S}\cdot\text{cm}^{-1}$), melting point (3498 K) and chemical stability in contact with pure Fe, great resistance to corrosion and oxidation (over 1100 °C), high specific strength, and good wear and creep resistance [130,131]. However, this compound exhibits poor sinterability due to its strong ionic and covalent bonds, low self-diffusion

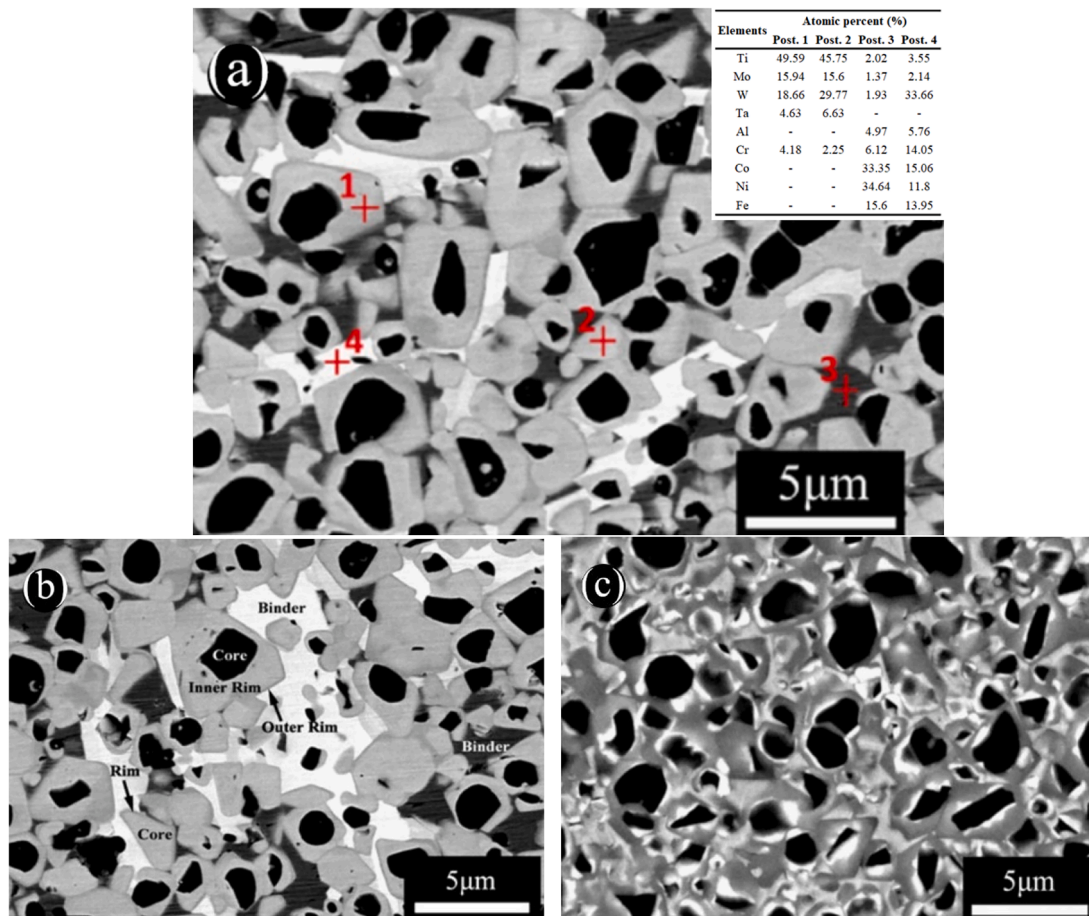


Fig. 10. Microstructure images of the Ti(C,N)-based cermets synthesized in the studies of Zhu et al. [128,129]. (a) Backscattering SEM of 50 wt% Ti(C_{0.7}N_{0.3}) – 25 wt% WC – 10 wt% (Mo₂C + TaC) – 15 wt% AlCoCrFeNi; (b) SEM of 42 wt% Ti(C_{0.7}N_{0.3}) – 25 wt% WC – 10 wt% Mo₂C – 8 wt% TaC – 15 wt% AlCoCrFeNi; SEM of 42 wt% Ti(C_{0.7}N_{0.3}) – 25 wt% WC – 10 wt% Mo₂C – 8 wt% TaC – 15 wt% NiCo. Reproduced with permission of Elsevier.

coefficient, and the presence of an O-rich layer (TiO₂ and B₂O₃) on its surface. Additionally, this ceramic has a high sintering temperature (over 2000 °C) and exhibits forms secondary brittle borides, leading to a low fracture toughness of ~5 MPa·m^{1/2} on its monolithic form, which limits its use in engineering applications [132–134].

To improve the performance of TiB₂-based cermets, several authors have employed HEAs as a sintering aid to enhance the composite densification and mechanical properties, whose main results, in terms of microstructural features and mechanical properties, are summarized in Table S3 of the Supplementary Material. Besides, synthesis route and cermet composition are listed too.

Yang et al. [135] studied the effect of sintering temperature and initial TiB₂ particle size on the microstructure and mechanical properties of TiB₂-12wt.%CoCrFeNi cemented carbide. It was observed that regardless of the sintering temperature, the composites fabricated with an initial ceramic particle size of 45 and 20 μm exhibited a microstructure composed by TiB₂, Ti(O,C,N), Cr₃B₄ and FCC solid solution, reaching a densification and Vickers hardness lower than 86 % and 5.8 GPa, respectively. When the initial ceramic particle size is 3 – 5 μm, the Cr₃B₄ secondary boride is not observed in the microstructure and the increase in temperature from 1400 to 1500 °C increases the densification and hardness but decreases the fracture toughness, from 94 %, 6.01 GPa and 7.7 MPa·m^{1/2} to 95.3 %, 6.84 GPa and 6.9 MPa·m^{1/2}, respectively. A further increase in temperature does not improve the mechanical properties and the awful combination of mechanical properties is mainly attributed to the low coverage ratio of the metallic binder in the cermet.

In contrast, Yang et al. [134] investigated the effect of the sintering

temperature on the microstructure and mechanical properties of TiB₂-5wt.%FeNiTiAl cermet, compared to the pure TiB₂ sintered at 1800 °C, the incorporation of the HEA as metallic binder increases the densification of the samples even at lower sintering temperature, reaching over 95 % of relative density in contrast to the 76.8 % achieved by the pure TiB₂. The consolidated samples were composed of TiB₂ ceramic phase, Ti(O, C, N), FCC metallic binder, Al₂O₃ and M₂B secondary borides formed by the reaction between the ceramic particles with Fe and Ni contained in the binder. As the temperature increases from 1200 to 1500 °C, the content of brittle secondary borides decreases from 3.8 to 1.2 wt%, however, the fracture toughness increases from 3.9 to 6.1 MPa·m^{1/2} due to the grain refinement and the plastic behavior of the metallic binder. The best combination on mechanical properties were attained by sintering at 1300 °C, achieving 97.3 % of densification, 21.1 GPa of Vickers hardness, 5.51 MPa·m^{1/2} of fracture toughness and 460.9 GPa of elastic modulus. If compared with those reported in [135], the higher hardness relays on the superior densification attained with FeNiTiAl as sintering aid, meanwhile the lower fracture toughness was attributed to the presence of secondary brittle borides. Nevertheless, both authors achieved a higher toughness in contrast to that of monolithic TiB₂ (5.2 MPa·m^{1/2}) [136], TiB₂-33wt.%CoTiAl (4.7 MPa·m^{1/2}) and TiB₂-20wt.%FeNi (5.5 MPa·m^{1/2}) [137], proving the better toughening effect of the HEA in contrast to the conventional metallic binders.

The TiB₂-5wt.%CoCrFeNiAl system was analyzed by, the effect of the sintering temperature on the mechanical properties was investigated by Zhang et al. [138], reporting that the microstructure was composed by an FCC solid solution, TiB₂ ceramic phase and an amorphous phase homogeneously distributed along the grain boundary of the TiB₂

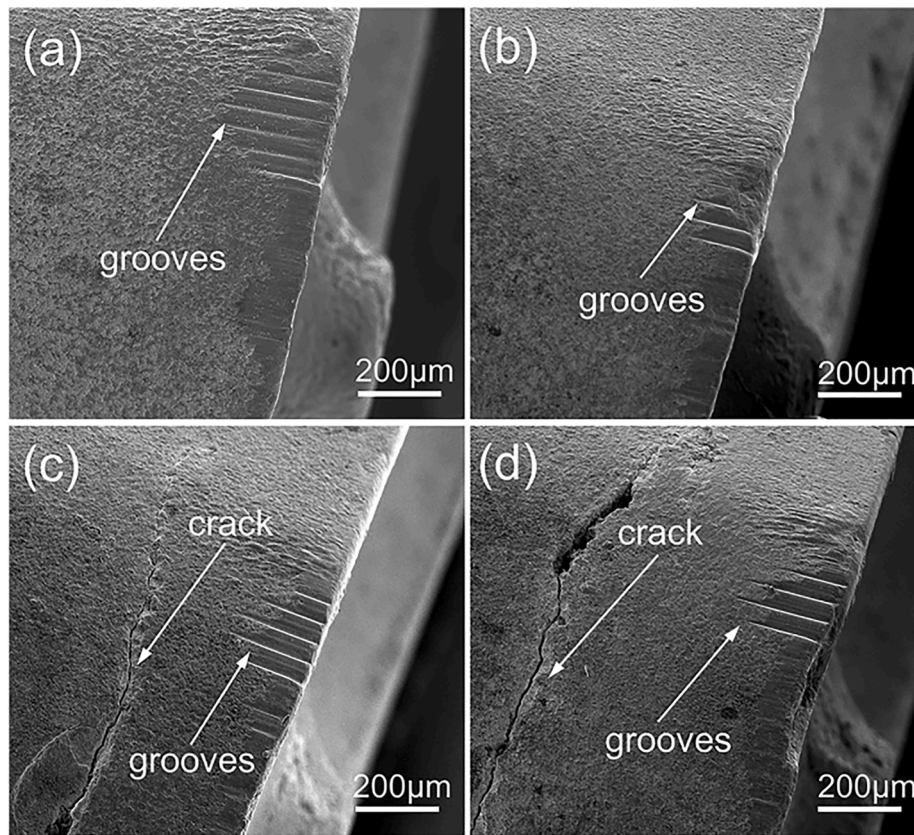


Fig. 11. Flank wear morphologies of (61 wt% - x)Ti(C,N)-15wt.%CoCrFeNi-18 wt%WC-6wt.%Mo2C-xNbC cermet inserts after cutting GCr15 bearing steel for 30 min: (a) x = 0 wt%; (b) x = 3 wt%; (c) x = 6 wt%; (d) x = 9 wt% [125]. Reproduced with permission of Elsevier.

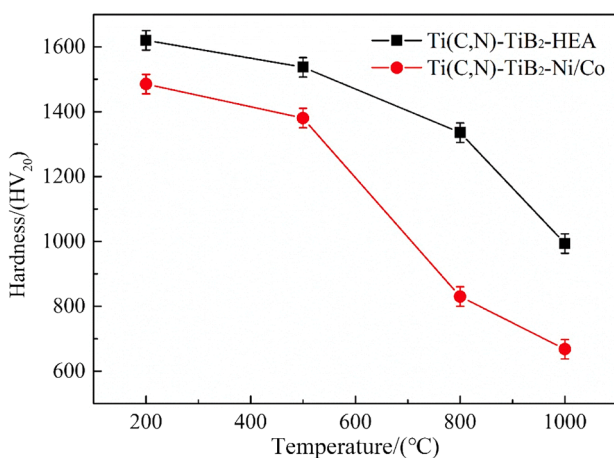


Fig. 12. High temperature hardness of the Ti(C,N)-TiB₂-FeCoNiCrAl and Ti(C,N)-TiB₂-Ni/Co cermets sintered at 1500 °C with 22.5 wt% of TiB₂ and 10 wt% of binder [120] Reproduced with permission of Elsevier.

particles and observing that as the sintering temperature increases from 1500 to 1650 °C the relative density, Vickers hardness and TRS values successfully increases from 95.5 %, 18.11 GPa and 478.7 MPa to 99.7 %, 23.12 GPa and 820 MPa, respectively. However, a further increase in the temperature slightly decreases the mechanical properties, and the best performance is reached when the sintering temperature is 1650 °C. This was later confirmed by Li et al. [139] whose studied microstructure and mechanical properties of TiB₂-5 wt.%CoCrFeNiAl sintered at 1650 °C, reporting the same microstructural composition and same values for the mechanical properties. The combination of nanocrystalline-amorphous

microstructure agrees with the so called “supra-nano-dual-phase structure” (SNDP) and this composite has become the first cermet with this kind of structure used as a binder phase. The better densification, hardness and flexural strength in comparison to those reported in [134,135,140] relies on the good wettability between the metallic and ceramic phase, the absence of secondary brittle borides and the excellent mechanical properties of CoCrFeNiAl with a SNDP structure [138].

The employment of CoCrFeNiAlTi HEA as metallic binder was reported in [141–143]. Fu et al. [142,143] analyzed the effect of the binder content and milling time on the microstructure and mechanical properties of TiB₂-CoCrFeNiAl fabricated using the C-coated precursors method (CCPM) to reduce the production cost and oxide rich layer present on the surface of TiB₂ ceramic particles. The authors reported that the implementation of an additional milling stage after the mechanical alloying process modifies the microstructure from FCC, TiB₂, Al₂O₃ and Ti₂O₃, to one containing FCC, TiB₂ and Al₂O₃, since reducing the particle size increases the reactivity between oxide impurities and Al dissolved in the metallic binder. Increasing the binder content from 5 to 20 wt% can effectively increase the densification but reduce the Vickers hardness, from 82 %, and 12.1 GPa to 86.5 % and 13.2 GPa, respectively. In the same way, conducting an additional milling stage of 2h effectively improved the densification and the Vickers hardness regardless of the metallic content. A further increase in the time of the additional milling stage resulted in negligible increase of the densification. The best combination of mechanical properties was attained with a 10 wt% of HEA binder, achieving a 97 % of densification with 17.5 GPa of Vickers hardness and 12.8 MPa·m^{1/2} of fracture toughness.

Similarly, Ji et al. [141] studied the effect of the sintering temperature on the mechanical properties of TiB₂-5wt.%CoCrFeNiAlTi cermet, reporting that independently the sintering temperature, the microstructure was composed by TiB₂, FCC solid solution, Al₂O₃, Ti(C, N, O)

and an amorphous phase. The increase in temperature from 1400 to 1600 °C effectively increases the densification, Vickers hardness and flexural strength from 96 %, 20.4 GPa and 540 MPa to 99.12 %, 23.11 GPa and 800 MPa, respectively. However, a further increase in this variable is detrimental for the mechanical properties and the best performance was achieved by the cemented carbide sintered at 1600 °C, exhibiting a 99.12 % of densification, 23.56 GPa of Vickers hardness and a flexural strength of 800 MPa. The present cermet had highly superior mechanical properties compared to the TiB₂-AlN cermet fabricated by Li et al. [144] or the TiB₂-Ti cemented carbide fabricated by Zhang et al. [145], attributed to the improvement in bulk densities, the excellent physical compatibility between the metallic binder and the reinforcement phase and to the presence of Ti and Al in the binder composition.

Finally, Zhao et al. [146] studied the effect of binder content on the densification and mechanical properties of TiB₂-CoCrFeNiTi_{0.5}Mn_{0.5} cermet, determining that every cermet was constituted by TiB₂, TiO, Ti₉O₁₇ and a FCC solid solution. Increasing the binder content from 0 to 10 wt% increases the densification and flexural strength from 85.5 % and 90.44 MPa to 99.1 % and 427.7 MPa, respectively. The cermet hardness increases only up to the incorporation of 7.5 wt% on metallic content and a further increase results detrimental for this mechanical property, reducing the Vickers hardness from 22.26 to 21.33 GPa. When the binder content is 10 wt% the cermet reaches the optimal combination between mechanical properties, reporting a 99.1 % of densification, 427.7 MPa of flexural strength and a Vickers hardness of 21.33 GPa, this results are somewhat similar to that reported by Fu et al. [142,143] and slightly higher hardness was achieved compared to that obtained by Yang et al. [134] with the TiB₂-5wt.%FeNiTiAl cermet sintered at 1300°C. However, these mechanical properties are completely lower than the obtained by Ji et al. [141], whose reported a 99.12 % of densification, 23.5 GPa of Vickers hardness and 800 MPa of bending strength for the cermet with better performance (TiB₂-5wt.%CoCrFeNiAlTi sintered at 1600 °C).

As could be seen, TiB₂-HEA cermets possessed superior mechanical properties in comparison with several conventional TiB₂-based composites [144,147], which makes the multicomponent alloy a suitable binder option to achieve the most advantageous combination between microstructure and mechanical performance. However, the performance of the TiB₂-HEA cermets is poorer in comparison to the WC-HEA and Ti (C,N)-HEA cermets, so further investigations are required to improve the performance of this composites in order to be a suitable candidate to replace the conventional WC-Co cemented carbides.

2.4. Other hard phases

Other ceramic phases have been studied as the hard phase of cermets bonded by HEAs. NbC has a comparable hardness (19.6 GPa) with WC, VC and TaC, high melting point (3600 °C) [148], and lower density (7.81 g/cm³) than WC [149]. Alternatively, Fe-based borides have attracted a lot of attention owing their technological applicability as hardening agent in steels [150], hard protective coating due to their high chemical and wear resistance [151], and as important shielding materials in nuclear reactors. Nevertheless, this compound also exhibits a relatively low melting point (1923 K), low thermal conductivity (15 Wm⁻¹K⁻¹), fracture toughness (1.2 – 2.8 MPa·m^{1/2}), Young's modulus (267 GPa) and slightly lower Vickers hardness (12 – 16 GPa), especially in comparison to the ceramic phases discussed above [152]. Table S4 (Supplementary Material) presents a summary of mechanical properties of HEAs-containing cermet employing these ceramic compounds as hard phase.

In this context, Shao et al. [153] fabricated the NbC-30vol.%CoCrFeNiMn via uniaxial pressing and LPS at different temperatures. The authors discovered that independently the sintering temperature, the cermet was composed by NbC, and a FCC solid solution and a M₂₃C₆ carbide reaching a relative density about 90 %, concluding that sintering temperature had no effect on the densification during sintering and the

low relative densities may be related to the poor wettability between the ceramic and binder phase. As the temperature rises from 1400 to 1550 °C, the average ceramic particle size increases from 4.8 μm to 14 μm and the hardness as well as the TRS decreases from 5.796 GPa and 497.13 MPa to 5.335 GPa and 359.45 MPa, respectively. The average particle size is lower than that of NbC-30vol.%Ni fabricated under the same conditions because the activation energy for NbC grain growth in HEA (696.6 kJ/mol) is significantly higher than that in Ni (352.4 kJ/mol) and those of conventional cermets with Fe [154], Co [154] and Cu [155] binder. The best performance was obtained by the NbC-30vol.% HEA sintered at 1400 °C but its Vickers hardness is lower than the cermet (WC-30vol.%HEA) obtained by Velo et al. [62] with the same amount of binder phase and fabricated via cold isostatic pressing and sintered at 1450 °C, that exhibited in all cases a hardness value over 9.87 GPa.

Recently, investigations on the field of high-entropy cermets have been made to determine if composites including FeB as reinforcement phase provide suitable performance to be used directly as a cermet or to be deposited on the materials surface as a coating. Xie et al. [156] synthesized the FeB-(12wt.%CoCrFeNiAl_{0.25}+10wt.%Mo) cermet via mechanical alloying and SPS at 1300 °C for 5 min. The results showed that the composite was composed by undissolved Mo + (Fe, Al, Ni, Co, Cr)₂B + (Fe, Al, Ni, Co, Cr)₂B with a relative density of 92.36 % and a Vickers hardness value between 14.3 and 14.8 GPa, higher than that obtained by previous works mainly because of the higher density and the fabrication process. However, as the fracture toughness was not investigated it cannot be possible to conclude if this composite is suitable to be used as cutting tool or drilling operations, and further studies have to be made.

On the other hand, Xie et al. [156–158] has been studied FeB-based HEA cermets as coatings deposited by AC-HVOF on the 316L stainless steel surface to improve its corrosion resistance in molten zinc (discussed in the Oxidation behavior of), a worldwide problem in the galvanizing industry [159]. This ceramic is less expensive than WC, possess low wettability with the liquid phase [160], high hardness (20.59 GPa) [161] and a thermal expansion coefficient (23 × 10⁻⁶ 1/K) [162] close to that of 316L stainless steel (19.3 × 10⁻⁶ 1/K) [163]. The results showed that using 12 wt% of CoCrFeNiAl_{0.25} as binder aid, the coating with a thickness of 375 μm presented a low Vickers hardness of 8.64 GPa due to the resultant porosity after the HVOF deposition and the resulting microstructure was composed by (Fe, Al, Ni, Co, Cr)₂B + (Fe, Al, Ni, Co, Cr)₂B due to the transformation of FeB into Fe₂B and the dissolution of HEA elements into the carbides. The coating thermal expansion coefficient was 12 × 10⁻⁶ 1/K, smaller than that of low C WC-Co (6.8 × 10⁻⁶ 1/K), WC-Co (7.2 × 10⁻⁶ 1/K) or Mo-CoCr (9.2 × 10⁻⁶ 1/K) [163], which may lead to fewer cracks during the thermal shock experiments. The abrasion experiments employing a rubber wheel test determined that the wear resistance of the coated stainless steel was almost twice as that of uncoated steel, resulting in a mass loss of 57.1 and 33.5 mg in contrast to the 111.0 and 83.6 mg for the coated and uncoated 316L SS after 200 and 1200 revolutions, respectively. Adding 10 wt% of Mo to the binder phase increased the hardness of the coating, varying between 10.04 and 10.55 GPa and improved the coating toughness because after the shock thermal test the first microcrack on the surface coating appeared after 37 shock thermal cycles in contrast to the 32 cycles for the FeB-12wt.% CoCrFeNiAl_{0.25}, indicating that Mo effectively reduced the brittleness of the coating. Increasing the binder content to 30 wt% of CoCrFeNiAl_{0.25} improved the coating wear resistance compared to the FeB-12wt.%HEA, decreasing the mass loss in 46.16 and 49.33 % after 200 and 1200 revolutions, respectively. After 1200 revolutions, the coating presented many obvious grinding pits and the river sand used in the rubber wheel abrasion test was embedded in defective locations of the coating, causing powder particles on the surface of the coating to peel off during the abrasive wear process and form grind pits, together with the many furrows observed in the surface of the 316L SS, corresponding to the typical form of wear observed for plastic materials. The Vickers hardness

of FeB-30 wt.%HEA varies between 8.11 and 8.42 GPa, like that obtained by the FeB-12wt.%HEA with a fracture toughness value varying between 5.27–5.89 MPa·m^{1/2}.

2.5. Hardening and toughening mechanisms in HEA-cermets

Continuous efforts to enhance hardness and toughness, with the goal of achieving an optimal balance between mechanical strength and toughness, have led to the use of high-entropy alloys as binders. These properties can be further improved by incorporating various elements that influence the hard phase, not only enhancing strength and toughness but also improving the wettability of the binder on the hard particles during liquid-phase sintering. This reduces coalescence and promotes a more uniform distribution of the ceramic particles [99,102].

Compared to traditional cermets, the higher density achieved by HEA-cermets, resulting from improved wettability and bonding between the metallic binder and ceramic particles, leads to enhanced hardness and toughness [120]. As mentioned by [142], despite the similar Vickers hardness values between Ni (4–5 GPa) and TiNiFeCrCoAl HEA (4 GPa), the increased contiguity contributes to the overall hardness due to the greater rigidity from the TiB₂-TiB₂ contacts. This is attributed to the higher density of the TiB₂-HEA cermet.

The reduction in ceramic grain size has also been identified as a key strengthening and toughening mechanism. The low solubility of the ceramic phase in the metallic binder results in smaller grain sizes, leading to enhanced grain boundary strengthening in accordance with the Hall-Petch relationship. Grain refinement further improves fracture toughness, as fine ceramic-ceramic grain boundaries possess higher interfacial energy, reducing the potential for crack propagation through intergranular sites. Consequently, a fine grain structure with uniform size distribution in the ceramic phase increases crack deflection and extends the fracture path, allowing for greater energy dissipation during crack propagation [164–167]. Therefore, inhibiting crack extension improves the fracture toughness of HEA cermets [81].

Another strengthening mechanism identified is solid solution strengthening. Liu et al. [110] reported that the high strength of TiC-MoVWNBtTa cermets is primarily due to this mechanism. The partial dissolution of the ceramic phase into the metallic binder further enhances the solid solution strengthening effect already present in the high-entropy binder [128,129]. However, the crystalline structure of the binder phase also plays a critical role in determining the composite's toughness. While BCC-structured HEAs generally exhibit high yield strength and limited plasticity, FCC-structured HEAs are characterized by greater plasticity and relatively lower yield strength. Identifying additional toughening mechanisms, such as ductile phase toughening, given by the high plasticity exhibited by FCC-structured HEAs [44,134].

The complex precipitation hardening mechanisms can be activated in systems such as WC-NiCoCrTiAl [60,90]. The resulting microstructure comprises a combination of the WC ceramic phase, the metallic binder, the (Ti_xW_{1-x})C complex carbide formed through the interaction between the ceramic phase and the metallic binder, aluminum-rich oxides (Al₂O₃) generated by the reduction of less stable oxides present in the powder mixtures, and γ -type precipitates [90]. The authors reported that the precipitation hardening cycle does not result in any measurable embrittlement of the binder phase, despite a hardness increase of 15%. However, crack initiation sites are linked to accumulations of alumina particles and pores. Preventing the formation of secondary brittle phases during the sintering process serves as a toughening mechanism, as their presence can negatively impact the fracture toughness of the composite [134]. Elements such as titanium can help prevent the formation of secondary brittle borides in TiB₂-based cermets. The synergistic effect of using Fe-Ni-Ti-Al metallic elements as sintering aids to improve the toughness of TiB₂ ceramics is superior to the addition of only Fe-Ni and titanium [134].

Finally, the remaining mechanisms contributing to high fracture toughness identified in HEA-based cermets are analogous to those found

in WC-Co composites. These mechanisms include a combination of crack branching, crack bridging, and grain pull-out [168,169]. In crack bridging, the HEA binder undergoes necking to either a point or a line as the crack propagates through the binder phase. This necking increases the total surface area, thereby leading to greater energy absorption and improved resistance to crack propagation [86]. As a result, the opening of the crack behind the tip is restrained, which aids in the enhancement of toughness [43]. Furthermore, the pull-out of certain ceramic grains at the ceramic/HEA interface is another energy-consuming process that enhances the toughness of the composite [89].

2.6. Constituent elements effect

Table 7 summarizes the individual effect of the constituent elements of the HEA used as a binder for the fabrication of cermets. One of the most important aspects is the stability of FCC or BCC solid solutions. As can be seen in Table 7, the addition of BCC elements, such as Cr, Mo, W, may induce the precipitation of secondary BCC solid solutions [69,93]. This same effect applies for other non-bcc elements, such as Al (despite of its FCC lattice structure in the pure state) [84] or Co [74], whose content may induce the transformation of the binder microstructure into a fully BCC one. These changes will impact of course the mechanical performance of the cermet, since BCC phases tend to exhibit poorer fracture toughness than FCC phases, accompanied by an enhance on their yield and ultimate strength. For example, the WC-20wt.% AlCoCrFeNiTi cermet achieved the best combination of mechanical properties (23.12 GPa of hardness, 12.1 MPa·m^{1/2} of fracture toughness and 5420 MPa of compression strength) among the cermets considered in this section, whose microstructure was precisely constituted by WC grains bonded by a BCC metallic matrix [56]. Other elements with a FCC lattice structure in their pure form at room temperature, such as Ni or Cu, would promote the formation of FCC phases.

Besides of the FCC-BCC stability effect of the binder constituent elements, these may have additional effects on microstructure. Cu-containing HEAs may present a secondary Cu-rich FCC solid solution as was reported in [74,84,87]; this same phenomenon was reported by Mueller-Gruntz et al. [76] studying WC-Al_xCoCrCuFeNi cermets. In this case, despite that Cu promotes FCC phases, its positive enthalpy of mixing regarding the rest of constituents of the alloy, as well as its lower melting point, promotes its segregation. In the case of Mn, it may conduct to the formation of pores in the microstructure, because of its high vapor pressure that causes its sublimation at elevated sintering temperatures according to the authors [170,171]. On the other hand, the addition of Al resulted in some cases in the formation of Al-rich oxides. It is recommendable to analyze if the effect of this oxide is detrimental to the alloy performance – not only in terms of mechanical properties, but also considering oxidation and corrosion behavior. On the other hand, it is also possible that the consumption of Al into oxide particles or intermetallic phases (such as Ni₃Al in [90]), causes a depletion of Al in the main solid solution, lower than that required to destabilize the FCC solid solution, that may explain the absence of BCC phases in [60,90].

A relevant aspect regarding microstructure and performance of cermets concerns the formation of complex carbides. FeCoNi-based binders may present the formation of η carbides, that despite having a detrimental effect over toughness, they have conducted to superior hardness values. These carbides have been reported as isolated carbide particles [68], as well as forming a core-rim structure with WC particles [62]. Other complex carbides, such as Co₃W₉C₄, Cr₇C₃, and Ti_{0.8}W_{0.2}C have been reported too, whose stability will depend on the content of these carbide former elements, the C content of the cermet, and the C window as well. Mo, on the other hand, has been reported as an inhibitor of the Cr₇Cr₃ formation because it reduces the carbide stability and changes the carbide formation sequence [172]. Other elements may affect the C window too in different manners: for example, the C window became wider with Ni additions but narrower with Fe additions [67,68]. When combined Fe, Ni and Co even larger C windows are obtained [5,30],

Table 7
Effect of constituent elements of the HEA binder on the cermet microstructure.

Element	Effect
Fe	<ul style="list-style-type: none"> - Enhances the sinterability of TiB₂-based cermets but promotes brittle borides such as M₂B and M₂₃B₆. - Shifts the lower limit of carbon window upwards due to the formation of η phase.
Co	<ul style="list-style-type: none"> - Inhibits grain growth but has a high tendency for carbide formation. - Enhance the toughness, corrosion resistance, and mechanical properties of the composite. - Forms secondary brittle borides (M₂B, M₂₃B₆). - Retain the carbon content during sintering due to its moderate solubility and excellent wettability on WC.
Cr	<ul style="list-style-type: none"> - Promotes Cr-rich carbide formation (M₇C₃). - Increases corrosion resistance, mechanical properties, and wettability on TiB₂-based cermets. - Forms secondary brittle borides (M₂B, M₂₃B₆). - Shift the lower limit of carbon window upwards due to the formation of η phase. - Enhance BCC phase formation.
Ni	<ul style="list-style-type: none"> - Dissolves in the hard phase in Ti(C,N)-based cermets. - Enhance toughness of the composite. - Improve the oxidation resistance at high temperature. - Lowers the sintering temperature of TiB₂ but forms brittle borides such as M₂B and M₂₃B₆. - Shifts the lower limit of the carbon window to lower carbon contents and the width of the two-phase region increases - Enhance FCC phase formation.
Al	<ul style="list-style-type: none"> - Promotes γ' precipitation and Al-rich oxides formation. - Improve hardness, red hardness and corrosion resistance at elevated temperatures. - Promotes phase segregation and formation of intermetallic compounds. - Lattice straining effect and destabilize the FCC structure when dissolved in FCC HEA. - Prevents formation of secondary brittle borides. - Inhibits Cu-rich phase with poor corrosion performance and reduces the Cr₂O₃ phase.
Cu	<ul style="list-style-type: none"> - Enhance FCC phase formation. - Tends to segregate in the interdendritic regions.
Mo	<ul style="list-style-type: none"> - Increases the corrosion resistance, although there is a slight decrease in density. - Slightly increases the toughness. - Promotes BCC phases.
Mn	<ul style="list-style-type: none"> - Increases the hardness and yield strength of the composite. - Enhances the sinterability and refines the microstructure of TiB₂ cermets. - Tendency to sublime during the liquid sintering process promoting pores formation
Ti	<ul style="list-style-type: none"> - Enhances the sinterability of TiB₂-based cermets but forms brittle borides such as M₂B and M₂₃B₆. - High levels promote the formation of secondary phases as sigma, laves among others. - Prevents formation of secondary brittle borides. - Dissolves in the hard phase in Ti(C,N)-based cermets.
V	<ul style="list-style-type: none"> - Allows to maintain the original mechanical properties but reduces the sinterability - Promotes BCC phases. - Dissolves in the hard phase in Ti(C,N)-based cermets.
Bi	<ul style="list-style-type: none"> - Used as soft dispersoid in HEA matrix because it usually does not form intermetallic phases with many elements

displacing the inferior and superior limit towards even higher C contents than that reported in Fe-Ni alloys. ThermoCalc® simulations can be used to study the C window of WC-HEAs cermets, although experimental values are usually displaced toward higher C contents than those predicted by the software; nonetheless, this tool still can be useful at least as a first approach [70].

In the particular case of B-containing cermets, it has been observed the formation of secondary brittle borides with the addition of Co, Cr, Ni, Fe and Ti. On the other hand, for TiC-based cermets, it is not possible to establish clear guidelines for the design of the binder based on the current literature: since in most of the available studies the hard phase corresponds to a mixture of carbides, the individual effect of the elements cannot be distinguished. Nevertheless, it is already possible to identify that Cr, Ti, and V can dissolve into the hard phase and conduct

to rim-core structures.

3. Oxidation behavior of HEAs-containing cermets

Research conducted on cermets employing alloys such as Ni/Co [66] or intermetallics like Ni₃Al [173] as binders has demonstrated their potential for robust oxidation resistance. However, despite this promising behavior, there remains a scarcity of comprehensive information in this domain as well as in the involved mechanisms. Considering the investigation of HEAs as binders for cermets emerges as a fertile ground for exploration, given the limited existing literature on the high-temperature oxidation processes of cermets employing HEAs but also the promising properties that these alloys exhibit under extreme environments [174–176]. This section aims to review noteworthy studies that offer insights into the oxidation processes in cermets employing diverse systems, shedding light on the potential applications and optimization of these materials.

Zhu et al. [129] studied the early high-temperature oxidation behavior of Ti(C,N)-AlCoCrFeNi cermet (TiC_{0.7}N_{0.3}-15%WC-10%M₂C-TaC-15%AlCoCrFeNi) and comparing it with the commercial Ni-Co bonded one (TiC_{0.7}N_{0.3}-15%WC-10%M₂C-TaC-15%Ni-Co). In both cases the binder exhibited a FCC solid solution. To study their corrosion kinetics, the samples were exposed to static air between 800 and 1100 °C. Hence, an increase in mass was observed as the temperature and oxidation time increased. After oxidation at 800 °C, both cermets presented negligible mass gain (less than 0.6 mg/cm²). However, at 1000 °C, the Ni-Co cermet presented a mass gain of 2.98 mg/cm² meanwhile that of the HEA cermet was 0.55 mg/cm². Both materials presented a two-step reaction kinetics: an initial step of a pronounced oxidation up to 100 min, followed by a slower step. At 1100 °C, the authors obtained a parabolic constant rate of $4.34 \times 10^{-12} \text{ mg}^2 \cdot \text{cm}^{-4} \cdot \text{s}^{-1}$, in the HEA cermet, two orders of magnitude inferior to that of the Ni/Co cermet. All this evidence the superior performance obtained by replacing the conventional binder by the AlCoCrFeNi HEA.

Fang et al. [124] studied the oxidation behavior through thermogravimetry methods of the Ti(C,N)-based cermet with 10 wt% of Al_{0.3}CoCrFeNi as binder, aiming for a higher hardness and softening resistance respect the previous cermet by means of the reduction of the Al content. For comparison purposes, the authors also prepared a cermet under the same fabrication route but using the commercial Ni/Co binder instead of the HEA. Just like before, only FCC binder microstructures were obtained whether for the HEA and the commercial Ni/Co cermet. A similar behavior was observed in them: a slow oxidation at the beginning followed by a rapid increase in mass gain as well the temperature raised. Nonetheless, the superior oxidation resistance provided by the HEA was reflected in the thickness of the oxidation layers: in the case of the Ni/Co cermet a thickness of 3.43 μm was observed, meanwhile it only reached 1.73 μm in the case of the HEA cermet. The cross section image presented in Fig. 13 showed that the oxide layer produced in the HEA cermet is compact, stable, dense and adherent to the surface, in opposition to that of the commercial one which shows several defects such as pores or microcracks due to the residual stresses generated by thermal expansion mismatch between the oxide scale constituents and the base alloy. Then, the presence of defects acted as channels for diffusion of O, accelerating the oxidation process [177].

In a further study, Fang et al. [178] incorporated ZrO₂ whiskers in the initial mixture to improve the strength and toughness of the cermet at both room and high temperature. Table 8 summarizes the binder content and composition, and well as the content of ZrO₂ whiskers of the studied cermets. Corrosion experiments were performed by means of thermogravimetric studies as well. The same trend as in [124] was observed, first as the temperature increases the weight gain remains constant and then increases sharply to stabilize. The authors found that the oxidation mass gain of Ni/TiCN and Ni/ZrO₂/TiCN was higher than those of HEA/TiCN and HEA/ZrO₂/TiCN. This last presented the lowest mass gain between the studied samples (16.89 wt% at 1500 °C). A

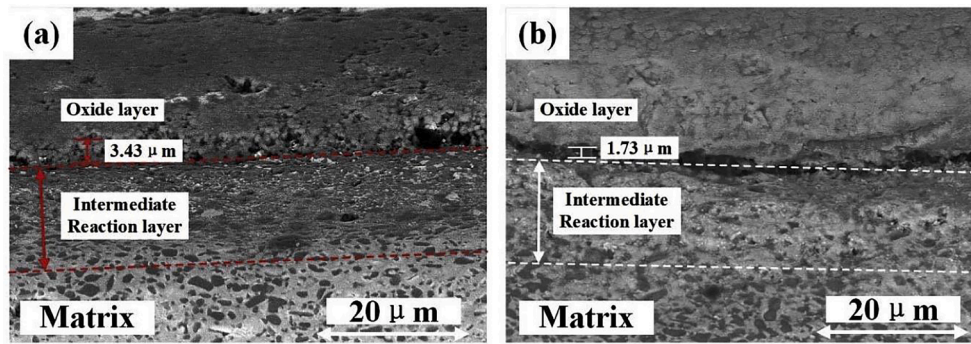


Fig. 13. Cross-sectional morphologies of cermet Ni/Co cermet and HEAs cermet after isothermal oxidation at 1000 °C for 4 h in static air: (a) Back scattering electron image from a polished section of cermet Ni/Co cermet; (b) Back scattering electron micrographs from a polished section of cermet HEAs cermet [124]. Reproduced with permission of Elsevier.

Table 8
Composition of Ti(C,N)-based cermet (wt. %) studied in [178].

Mark symbol	Content (wt. %)								
	Ti(C, N)	ZrO ₂	WC	TaC	Mo ₂ C	Ni	Co	Al _{0.3} CoCrFeNi	N
Ni/TiCN	70	0	10	5	5	8	2	0	
HEA/TiCN	70	0	10	5	5	0	0	10	
Ni/ZrO ₂ /TiCN	62.5	7.5	10	5	5	8	2	0	
HEA/ZrO ₂ /TiCN	62.5	7.5	10	5	5	0	0	10	

multilayer structure was observed after the oxidation process, consisting of an external oxide layer, an intermediate reaction layer, and the substrate. Regarding the morphology of the cracks, the researchers concluded that thanks to the dense and continuous oxide layer obtained with the HEAs cermets, the corrosion process is inhibited because they

do not allow the diffusion of O. Along with the above, it was observed that ZrO₂ whiskers effectively resulted in a better performance against corrosion. To quantify this analysis, the oxidation mass gain curves for holding at 1000 °C in air for 4h were studied. The analyzes indicated that a mass gain of 2.45 mg/cm² was obtained in the case of the HEA/ZrO₂/TiCN, meanwhile those of the HEA/TiCN, Ni/ZrO₂/TiCN, and Ni/TiCN cermets were 2.59, 6.11, and 6.53 mg/cm², respectively).

Fu et al. [179] studied the oxidation behavior of Ti(C,N)-TiB₂-AlCoCrFeNi cermets at three temperatures (800, 900, and 1000 °C) and employing different binder contents (6, 10, and 14 wt%). In this study was observed that the amount of binder has a great importance in the microstructure, which favors the mechanical properties and response to oxidation of the cermet. Indistinctly of the binder content, the mass increased with the temperature due to the formation of oxides such as TiO₂, alongside small amounts of Al₂O₃, FeTiO₃ and Al₂TiO₅. Between 800 and 900 °C the cermet with 10 wt% of HEA-Cermet has greater resistance to oxidation, but at 1000° the one with 14 wt% of HEA-Cermet was superior. This was associated to the higher number of metallic atoms able to diffuse to the surface, which will consume more O

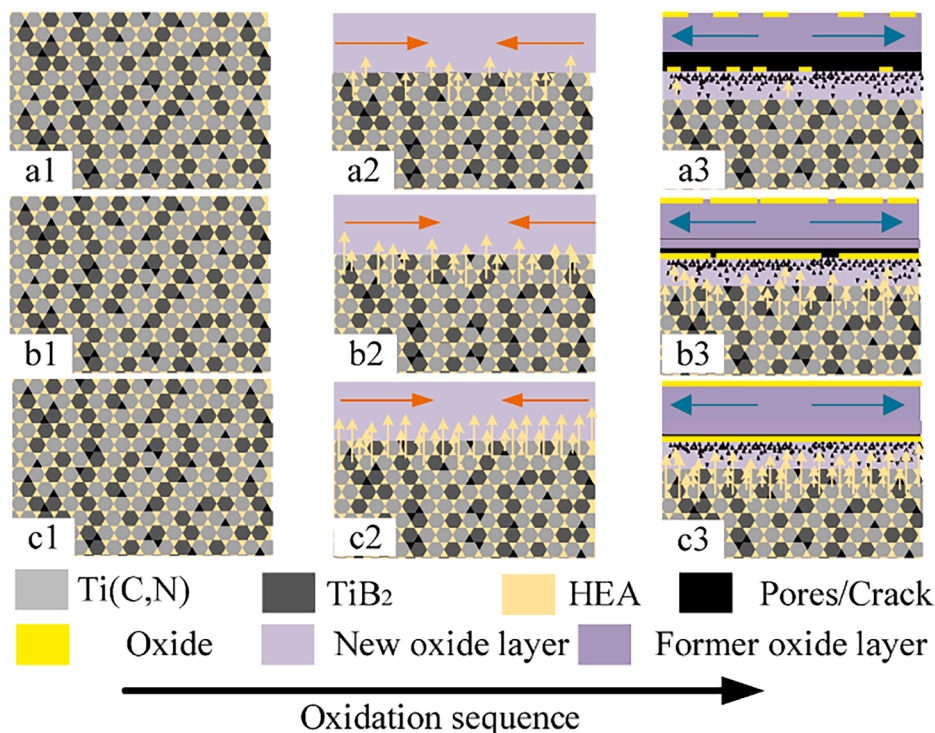


Fig. 14. Schematic diagram of the possible formation process for the laminated structure in the oxide layer (a) 6 wt%, (b) 10 wt%, (c) 14 wt% [179].

and form a dense oxide layer. A proposal for this mechanism is seen in Fig. 14: whereas the % of binder increases, the cracks gradually disappear and are replaced by an oxide layer – presumably, Al_2O_3 . On the other hand, as the binder content increases, the pores decrease and the density of the cermet increases; however, with 14 wt% of binder, it begins to segregate, which generates a decrease in properties such as hardness and tenacity fracture.

As can be appreciated from the previous results, the superior oxidation resistance of HEAs can be transferred to cermets containing HEAs as binders. Particularly, the addition of protective elements such as Al, Si, or Cr, can result in promising properties as have been observed in fully metallic HEAs. Nonetheless, it is absolutely evident the scarce literature already available regarding the oxidation performance of HEAs-containing cermet. Since the interaction between the cermet and the oxidation environments is highly dependent on the binder composition, and because of the complex effect of the composition and microstructure over oxidation behavior, further research is required in this field. This will be particularly needed for tailoring the HEA composition to improve the performance of the cermet.

4. Concluding remarks and future work

Due to the high cost of Co and its carcinogenic potential, there is a significant drive to develop alternative binders for WC-based cermets to replace them altogether. Due to the immense compositional space of HEA, the potential for finding new cost-effective HEA-ceramic combinations with high mechanical, wear and oxidation resistance is promising, but it requires intensive exploration. Apart from the vast amount of chemical compositions possible, another great challenge is to unify the tests performed and the results obtained as there is no single standard to evaluate and report mechanical properties and wear resistance. Especially in the case of wear resistance, the behavior of the sintered cermets will be highly dependent on the test conditions and wear mechanism, not being comparable two wear rates obtained under different testing conditions, so the purpose of this review is to provide an overview of the current state of the matter while carefully providing the details of how the results were obtained.

For most of the articles analyzed, the sintering temperature and process has a crucial role as there is a balance between the consolidation of the sintered cermet and the precipitation of deleterious phases and also the dissolution of the ceramic phase. So for each combination of HEA and ceramic, the analysis indicates that there is an optimal sintering procedure that optimizes the Vickers hardness, and transverse rupture strength (TRS) which translates to their wear behaviour.

Additionally, the review delves into alternative ceramic phases, such as niobium carbide (NbC) and iron borides (FeB), as reinforcing agents in cermets with HEA binders. The careful selection of these ceramic phases is driven by considerations of solubility and hardness, offering alternatives to conventional choices like WC. The incorporation of NbC and FeB introduces new dimensions to cermet design, expanding the range of materials available for tailoring properties to specific applications.

Based on the studies published so far, the following topics might help to further advance this field:

- **Optimization of HEA Compositions:** Tailoring the composition of HEAs in cermets to further enhance their performance remains a key area for investigation. Exploring variations in the types and ratios of alloying elements within the HEA matrix could yield materials with improved mechanical and thermal properties.
- **In-Depth Oxidation Studies:** The oxidation behavior of cemented carbides with HEA binders is an underexplored area. Future research should delve deeper into understanding the intricate mechanisms governing oxidation processes. This involves studying the impact of HEA composition, microstructure, and environmental factors on the formation and stability of oxide layers.
- **Advanced Processing Techniques:** Investigating novel processing techniques for fabricating HEA-containing cermets could open new possibilities. Techniques such as spark plasma sintering, additive manufacturing, or hybrid methods may offer advantages in terms of improved densification, tailored microstructures, and cost-effective production.
- **Mechanical Property Optimization:** While the mechanical properties of TiB_2 -HEA cermets show promise, further efforts can be directed toward optimizing parameters such as hardness, fracture toughness, and wear resistance. Systematic studies on the effects of sintering conditions, binder content, and secondary reinforcements can guide the development of cermets with superior mechanical performance.
- **Exploration of Additional Reinforcement Phases:** The incorporation of alternative ceramic phases beyond TiB_2 , such as carbides like NbC or borides like FeB, presents an intriguing avenue for investigation. Assessing the mechanical and thermal properties of HEA-containing cermets with diverse reinforcement phases could broaden their applicability in various industrial contexts.
- **Corrosion Resistance Studies:** The interaction between HEA-containing cermets and corrosive environments is an area warranting attention. Systematic studies on corrosion resistance, especially in aggressive conditions relevant to industrial applications, can inform the development of cermets for specific end-use scenarios.
- **Multiscale Modeling and Simulation:** Employing advanced computational tools for multiscale modeling and simulation can provide a deeper understanding of the complex relationships between microstructure, composition, and performance. Computational studies can guide experimental efforts and accelerate the discovery of optimal HEA compositions and processing conditions.
- **Application-Specific Investigations:** Tailoring HEA-containing cermets for specific applications, such as cutting tools, drilling operations, or wear-resistant coatings, requires targeted investigations. Future research should address the performance requirements of these applications and fine-tune cermet properties accordingly.

In conclusion, the synthesis of existing knowledge and identification of research gaps present exciting opportunities for future exploration in the realm of HEA-containing cermets. Addressing these avenues will not only advance fundamental understanding but also pave the way for the practical implementation of these innovative materials in diverse industrial applications.

CRedit authorship contribution statement

C. Madrid: Writing – original draft, Visualization, Investigation, Formal analysis, Data curation, Conceptualization. **C. Cáceres:** Writing – original draft, Visualization, Investigation, Formal analysis, Data curation, Conceptualization. **Víctor M. Jiménez-Arévalo:** Writing – original draft, Formal analysis, Data curation. **P. Martín:** Writing – review & editing, Writing – original draft, Visualization, Validation, Supervision, Project administration, Methodology, Investigation, Formal analysis, Conceptualization. **N. Araya:** Writing – review & editing, Writing – original draft, Supervision, Project administration, Methodology, Formal analysis, Conceptualization. **C. Aguilar:** Writing – original draft, Visualization, Investigation, Formal analysis, Data curation, Conceptualization.

Declaration of competing interest

The authors declare the following financial interests/personal relationships which may be considered as potential competing interests: Claudio Aguilar reports financial support was provided by National Agency for Research and Innovation. Pablo Martín reports financial support was provided by National Agency for Research and Innovation. If there are other authors, they declare that they have no known

competing financial interests or personal relationships that could have appeared to influence the work reported in this paper.

Acknowledgments

This work was funded by the Millennium Institute on Green Ammonia as Energy Vector—MIGA (ICN2021_023) supported by the Millennium Scientific Initiative and by FONDECYT n° 1230620, FONDECUIP n° EQM140095, Claudio Aguilar thanks the postgraduate Scholarship ANID n° 74220021. P. Martin gratefully acknowledges to ANID/Doctorado Becas Chile/2019-72200338. In addition, V. Jimenez-Arevalo is grateful for the support of the Vicerrectoria de Investigación, Innovación y Creación with the postdoctoral project DICYT N° 022442PC.

Appendix A. Supplementary data

Supplementary data to this article can be found online at <https://doi.org/10.1016/j.matdes.2024.113431>.

Data availability

Data will be made available on request.

References

- [1] J.R. Davis, *Metals Handbook*, Desk edition, 2nd ed., 1998.
- [2] L. Prakash, *Fundamentals and general applications of hardmetals*, Elsevier, 2014.
- [3] Z.Z. Fang, M.C. Koopman, H. Wang, Cemented Tungsten Carbide Hardmetal-An Introduction, in: *Comprehensive Hard Materials*, Elsevier, 2014; pp. 123–137. <https://doi.org/10.1016/B978-0-08-096527-7.00004-0>.
- [4] K. Schröter, *Hard metal alloys and process of making them*, USA Patent US 1549615A (1925) 3–4.
- [5] J. García, V. Collado Ciprés, A. Blomqvist, B. Kaplan, Cemented carbide microstructures: a review, *Int. J. Refract. Metals Hard. Mater.* 80 (2019) 40–68, <https://doi.org/10.1016/j.ijrmhm.2018.12.004>.
- [6] H. Saito, A. Iwabuchi, T. Shimizu, Effects of Co content and WC grain size on wear of WC cemented carbide, *Wear* 261 (2006) 126–132, <https://doi.org/10.1016/j.wear.2005.09.034>.
- [7] G.S. Upadhyaya, *Materials science of cemented carbides — an overview*, Mater. Des. 22 (2001) 483–489, [https://doi.org/10.1016/S0261-3069\(01\)00007-3](https://doi.org/10.1016/S0261-3069(01)00007-3).
- [8] J. Gurland, P. Bardzil, Relation of strength, composition, and grain size of sintered WC-Co alloys, *JOM* 7 (1955) 311–315, <https://doi.org/10.1007/BF03377497>.
- [9] H.E. Exner, J. Gurland, A review of parameters influencing some mechanical properties of tungsten carbide-cobalt alloys, *Powder Metall.* 13 (1970) 13–31, <https://doi.org/10.1179/pom.1970.13.25.002>.
- [10] A. Krawitz, E. Drake, Residual stresses in cemented carbides — An overview, *Int. J. Refract. Metals Hard. Mater.* 49 (2015) 27–35, <https://doi.org/10.1016/j.ijrmhm.2014.07.018>.
- [11] A.D. Krawitz, E.F. Drake, Residual Stresses, in: V. Sarin (Ed.), *Comprehensive Hard Materials*, Elsevier, 2014; pp. 385–404. <https://doi.org/10.1016/B978-0-08-096527-7.00013-1>.
- [12] S. Willersinn, H.-J. Bart, Reactive extraction and critical raw materials: industrial recovery of Tungsten, *Chem. Ing. Tech.* 89 (2017) 82–91, <https://doi.org/10.1002/cite.201600079>.
- [13] World Economic Forum; Global Battery Alliance, A Vision for a Sustainable Battery Value Chain in 2030, 2019. www.weforum.org.
- [14] L. Mancini, N.A. Eslava, M. Traverso, F. Mathieux, Assessing impacts of responsible sourcing initiatives for cobalt: insights from a case study, *Resour. Policy* 71 (2021) 102015, <https://doi.org/10.1016/j.resourpol.2021.102015>.
- [15] P. Wild, Lung cancer mortality in a site producing hard metals, *Occup. Environ. Med.* 57 (2000) 568–573, <https://doi.org/10.1136/oem.57.8.568>.
- [16] A. Linna, Exposure to cobalt in the production of cobalt and cobalt compounds and its effect on the heart, *Occup. Environ. Med.* 61 (2004) 877–885, <https://doi.org/10.1136/oem.2003.009605>.
- [17] R.K. Viswanadham, P.G. Lindquist, Transformation-toughening in cemented carbides: Part I. Binder Composition Control, *Metall. Trans. A* 18 (1987) 2163–2173, <https://doi.org/10.1007/BF02647089>.
- [18] B. Wittmann, Bernhard and Schubert, Wolf-Dieter and Lux, *Hardmetals with iron-based binder*, 2002.
- [19] S. Takeda, A metallographic study of the action of the cementing materials for cemented tungsten carbide, *Science Rept Tohoku Univ, Honda Anniv*, 1936, pp. 864–881.
- [20] H. Suzuki, T. Yamamoto, N. Chujo, Properties of WC-10%(Ni-Fe) Alloys, *J. Jpn. Soc. Powder Metall.* 14 (1967) 308–313, <https://doi.org/10.2497/jjspm.14.308>.
- [21] W. Schwarzkopf, Paul and Kieffer, Richard and Leszynski, *Cemented carbides*, Macmillan, 1960.
- [22] C. Agte, *Entwicklung der Hartmetalltechnik während der letzten Jahre in der Deutschen Demokratischen Republik*, *Neue Hütte* 9 (1957) 537–544.
- [23] D. Moskowitz, M.J. Ford, M. Humenik, High-strength tungsten carbides, *Int. J. Powder Metall* 6 (1970) 55–64.
- [24] J. Sun, J. Zhao, F. Gong, X. Ni, Z. Li, Development and application of WC-based alloys bonded with alternative binder phase, *Crit. Rev. Solid State Mater. Sci.* 44 (2019) 211–238, <https://doi.org/10.1080/10408436.2018.1483320>.
- [25] C. Liu, *Alternative Binder Phases for WC, Cemented Carbides* (2014).
- [26] A.F. Guillermet, An Assessment of the Fe-Ni-W-C Phase Diagram, *Int. J. Mater. Res.* 78 (1987) 165–171, <https://doi.org/10.1515/ijmr-1987-780301>.
- [27] C. Hanyaloglu, B. Aksakal, J.D. Bolton, Production and indentation analysis of WC/Fe-Mn as an alternative to cobalt-bonded hardmetals, *Mater Charact* 47 (2001) 315–322, [https://doi.org/10.1016/S1044-5803\(02\)00181-X](https://doi.org/10.1016/S1044-5803(02)00181-X).
- [28] Z. Nishiyama, *Martensitic transformation*, Elsevier, 2012.
- [29] S. Sevost'yanova, IN and Garms, AP and Gnyusov, SF and Kul'kov, Heat treatment and matrix composition effects on forming physical-and-mechanical properties of WC-(Fe-Mn-C) hard alloys, *Perspekt. Mater.* 4 (1998) 37–41.
- [30] W.D. Schubert, M. Fugger, B. Wittmann, R. Useldinger, Aspects of sintering of cemented carbides with Fe-based binders, *Int. J. Refract. Metals Hard. Mater.* 49 (2015) 110–123, <https://doi.org/10.1016/j.ijrmhm.2014.07.028>.
- [31] Z. Zhao, J. Liu, H. Tang, X. Ma, W. Zhao, Investigation on the mechanical properties of WC-Fe-Cu hard alloys, *J. Alloy. Compd.* 632 (2015) 729–734, <https://doi.org/10.1016/j.jallcom.2015.01.300>.
- [32] T.W. Penrice, Alternative binders for hard metals, *J. Mater. Shap. Technol.* 5 (1987) 35–39, <https://doi.org/10.1007/BF02833684>.
- [33] C.M. Fernandes, A.M.R. Senos, J.M. Castanho, M.T. Vieira, Effect of the Ni Chemical Distribution on the Reactivity and Densification of WC-(Fe/Ni/Cr) Composite Powders, *Mater. Sci. Forum* 514–516 (2006) 633–637, <https://doi.org/10.4028/www.scientific.net/MSF.514-516.633>.
- [34] Z. Zhao, J. Liu, H. Tang, X. Ma, W. Zhao, Effect of Mo addition on the microstructure and properties of WC-Ni-Fe hard alloys, *J. Alloy. Compd.* 646 (2015) 155–160, <https://doi.org/10.1016/j.jallcom.2015.05.277>.
- [35] A.V. Tumanov, Y.V. Gostev, V.S. Panov, Y.F. Kots, Wetting of TiC-Wc system carbides with molten Ni3Al, *Soviet, Powder Metall. Met. Ceram.* 25 (1986) 428–430, <https://doi.org/10.1007/BF00813961>.
- [36] V.S. Panov, M.A. Gol'dberg, Interaction of tungsten carbide with aluminum nickeline Ni3Al, *Powder Metall. Met. Ceram.* 48 (2009) 445–448, <https://doi.org/10.1007/s11106-009-9146-3>.
- [37] B. Huang, W. Xiong, Q. Yang, Z. Yao, G. Zhang, M. Zhang, Preparation, microstructure and mechanical properties of multicomponent Ni3Al-bonded cermets, *Ceram. Int.* 40 (2014) 14073–14081, <https://doi.org/10.1016/j.ceramint.2014.05.135>.
- [38] Y.X. Li, J.D. Hu, H.Y. Wang, Z.X. Guo, Study of TiC/Ni3Al composites by laser ignited self-propagating high-temperature synthesis (LISHS), *Chem. Eng. J.* 140 (2008) 621–625, <https://doi.org/10.1016/j.cej.2007.11.034>.
- [39] L. Liang, X. Q. Li, Y.Y. Li, Wear mechanisms of WC-10Ni3Al carbide tool in dry turning of Ti6Al4V, *Int. J. Refract. Metals Hard. Mater.* 48 (2015) 272–285, <https://doi.org/10.1016/j.ijrmhm.2014.09.019>.
- [40] X. Liu, L. Liang, X. Li, Y. Li, Abrasion wear behavior of WC-10Ni3Al cermet with plate-like triangular prismatic WC grains, *Ceram. Int.* 41 (2015) 5147–5158, <https://doi.org/10.1016/j.ceramint.2014.12.089>.
- [41] V.A. Tracey, Nickel in hardmetals, *Int. J. Refract. Metals Hard. Mater.* 11 (1992) 137–149, [https://doi.org/10.1016/0263-4368\(92\)90056-8](https://doi.org/10.1016/0263-4368(92)90056-8).
- [42] B. Cantor, I.T.H. Chang, P. Knight, A.J.B. Vincent, Microstructural development in equiatomic multicomponent alloys, *Mater. Sci. Eng. A* 375–377 (2004) 213–218, <https://doi.org/10.1016/j.msea.2003.10.257>.
- [43] J.-W. Yeh, S.-K. Chen, S.-J. Lin, J.-Y. Gan, T.-S. Chin, T.-T. Shun, C.-H. Tsau, S.-Y. Chang, Nanostructured high-entropy alloys with multiple principal elements: novel alloy design concepts and outcomes, *Adv. Eng. Mater.* 6 (2004) 299–303, <https://doi.org/10.1002/adem.200300567>.
- [44] Y. Zhang, T.T. Zuo, Z. Tang, M.C. Gao, K.A. Dahmen, P.K. Liaw, Z.P. Lu, Microstructures and properties of high-entropy alloys, *Prog. Mater. Sci.* 61 (2014) 1–93, <https://doi.org/10.1016/j.pmatsci.2013.10.001>.
- [45] C.-J. Tong, M.-R. Chen, J.-W. Yeh, S.-J. Lin, S.-K. Chen, T.-T. Shun, S.-Y. Chang, Mechanical performance of the AlxCoCrCuFeNi high-entropy alloy system with multiprincipal elements, *Metall. Mater. Trans. A* 36 (2005) 1263–1271, <https://doi.org/10.1007/s11661-005-0218-9>.
- [46] M.-R. Chen, S.-J. Lin, J.-W. Yeh, M.-H. Chuang, S.-K. Chen, Y.-S. Huang, Effect of vanadium addition on the microstructure, hardness, and wear resistance of Al0.5CoCrCuFeNi high-entropy alloy, *Metall. Mater. Trans. A* 37 (2006) 1363–1369, <https://doi.org/10.1007/s11661-006-0081-3>.
- [47] O.N. Senkov, S.V. Senkova, D.B. Miracle, C. Woodward, Mechanical properties of low-density, refractory multi-principal element alloys of the Cr-Nb-Ti-V-Zr system, *Mater. Sci. Eng. A* 565 (2013) 51–62, <https://doi.org/10.1016/j.msea.2012.12.018>.
- [48] O.N. Senkov, G.B. Wilks, J.M. Scott, D.B. Miracle, Mechanical properties of Nb25Mo25Ta25W25 and V20Nb20Mo20Ta20W20 refractory high entropy alloys, *Intermetallics (barking)* 19 (2011) 698–706, <https://doi.org/10.1016/j.intermet.2011.01.004>.
- [49] M.-H. Tsai, J.-W. Yeh, High-Entropy Alloys: A Critical Review, *Mater Res Lett* 2 (2014) 107–123, <https://doi.org/10.1080/21663831.2014.912690>.
- [50] E. Castle, T. Csanádi, S. Grasso, J. Dusza, M. Reece, Processing and properties of high-entropy ultra-high temperature carbides, *Sci. Rep.* 8 (2018) 8609, <https://doi.org/10.1038/s41598-018-26827-1>.

- [51] A. Ostovari Moghaddam, M. Sudarikov, N. Shaburova, D. Zhrebtsov, V. Zhivulin, I. Ashurali Solizoda, A. Starikov, S. Veselkov, O. Samoiloova, E. Trofimov, High temperature oxidation resistance of W-containing high entropy alloys, *J Alloys Compd* 897 (2022) 162733, <https://doi.org/10.1016/j.jallcom.2021.162733>.
- [52] C. Suryanarayana, *Mechanical Alloying and Milling* (2001), <https://doi.org/10.4150/kpmi.2006.13.5.371>.
- [53] P. Cavaliere, *Spark Plasma Sintering of Materials* (2019), <https://doi.org/10.1007/978-3-030-05327-7>.
- [54] P. Martin, C. Aguilar, J.M. Cabrera, A review on mechanical alloying and spark plasma sintering of refractory high-entropy alloys: Challenges, microstructures, and mechanical behavior, *J. Mater. Res. Technol.* 30 (2024) 1900–1928, <https://doi.org/10.1016/j.jmrt.2024.03.205>.
- [55] J.M. Torralba, P. Alvarado, A. García-Junceda, High-entropy alloys fabricated via powder metallurgy. A Critical Review, *Powder Metall.* 62 (2019) 84–114, <https://doi.org/10.1080/00325899.2019.1584454>.
- [56] P.F. Zhou, D.H. Xiao, T.C. Yuan, Comparison between ultrafine-grained WC–Co and WC–HEA-cemented carbides, *Powder Metall.* 60 (2017) 1–6, <https://doi.org/10.1080/00325899.2016.1260903>.
- [57] M.A. Ruiz-Esparza-Rodriguez, C.G. Garay-Reyes, I. Estrada-Guel, R. Martinez-Sanchez, Microstructural, Structural and Mechanical Behavior of WC-Based Hardmetals Bonded with High and Medium Entropy Alloys, *Microsc. Microanal.* 25 (2019) 1794–1795, <https://doi.org/10.1017/s143192761900970x>.
- [58] Q. Zou, Y. Dan, Y. Li, J. Xiong, Y. Luo, Effects of CoCrNiCuFe on microstructure and properties of WC cemented carbide, *In* (2020). <https://ssrn.com/abstract=4123304>.
- [59] P.L. Zhou, D.H. Xiao, P.F. Zhou, T.C. Yuan, Microstructure and properties of ultrafine grained AlCrFeCoNi/WC cemented carbides, *Ceram. Int.* 44 (2018) 17160–17166, <https://doi.org/10.1016/j.ceramint.2018.06.171>.
- [60] T. Soria-Biurrun, J. Navarrete-Cuadrado, L. Lozada-Cabezas, F. Ibarreta-Lopez, R. Martinez-Pampliega, J.M. Sánchez-Moreno, Microstructure, mechanical properties and fracture behavior of NiCoCrTiAl and FeNiCoCr new alternative binders for WC based hardmetals, *Int. J. Refract. Metals Hard. Mater.* 103 (2022), <https://doi.org/10.1016/j.ijrmhm.2021.105748>.
- [61] B. Cantor, Multicomponent high-entropy Cantor alloys, *Prog. Mater. Sci.* 120 (2021), <https://doi.org/10.1016/j.pmatsci.2020.100754>.
- [62] I.L. Velo, F.J. Gotor, M.D. Alcalá, C. Real, J.M. Córdoba, Fabrication and characterization of WC-HEA cemented carbide based on the CoCrFeNiMn high entropy alloy, *J. Alloy. Compd.* 746 (2018) 1–8, <https://doi.org/10.1016/j.jallcom.2018.02.292>.
- [63] F.Q. Li, Y. Bin Chen, L.Q. Li, Microstructures of surface modification layer on Q235 steel produced by laser melt injection of WC, *Trans. Nonferrous Metals Soc. China (Engl. Ed.)* 19 (2009), [https://doi.org/10.1016/S1003-6326\(10\)60108-2](https://doi.org/10.1016/S1003-6326(10)60108-2).
- [64] M.A. Ruiz-Esparza-Rodriguez, C.G. Garay-Reyes, I. Estrada-Guel, K.A. Garcia-Aguirre, J.C. Guia-Tello, J.M. Mendoza-Duarte, R. Martinez-Sanchez, Effect of Sintering Temperature in Tungsten Carbides Bonded with High and Medium Entropy Alloys, *Microsc. Microanal.* 28 (2022) 2802–2804, <https://doi.org/10.1017/s1431927622010571>.
- [65] M.A. Ruiz-Esparza-Rodriguez, C.G. Garay-Reyes, J.C. Guía-Tello, H.M. Medrano-Prieto, I. Estrada, R. Martínez-Sánchez, Study of densification, microstructure, and mechanical properties in WC-based hardmetals bonded with high and medium entropy alloys, *Microsc. Microanal.* (2020), <https://doi.org/10.1017/S1431927620024253>.
- [66] D. Dong, X. Xiang, B. Huang, H. Xiong, L. Zhang, K. Shi, J. Liao, Microstructure and properties of WC-Co/CrMnFeCoNi composite cemented carbides, *Vacuum* 179 (2020), <https://doi.org/10.1016/j.vacuum.2020.109571>.
- [67] C. Qian, Y. Liu, H. Cheng, K. Li, B. Liu, X. Zhang, The Effect of Carbon Content on the Microstructure and Mechanical Properties of Cemented Carbides with a CoNiFeCr High Entropy Alloy Binder, *Materials* 15 (2022), <https://doi.org/10.3390/ma15165780>.
- [68] C. Qian, Y. Liu, H. Cheng, K. Li, B. Liu, Effect of the carbon content on the morphology evolution of the η phase in cemented carbides with the CoNiFeCr high entropy alloy binder, *Int. J. Refract. Metals Hard. Mater.* 102 (2022), <https://doi.org/10.1016/j.ijrmhm.2021.105731>.
- [69] T. Soria-Biurrun, L. Lozada-Cabezas, F. Ibarreta-Lopez, R. Martinez-Pampliega, J.M. Sanchez-Moreno, Effect of chromium and carbon contents on the sintering of WC-Fe-Ni-Co-Cr multicomponent alloys, *Int. J. Refract. Metals Hard. Mater.* 92 (2020), <https://doi.org/10.1016/j.ijrmhm.2020.105317>.
- [70] T. Soria-Biurrun, L. Lozada-Cabezas, J. Navarrete-Cuadrado, F. Ibarreta-Lopez, R. Martinez-Pampliega, J.M. Sánchez-Moreno, Densification of WC-Fe-Ni-Co-Cr cemented carbides processed by HIP after sintering: effect of WC powder particle size, *Int. J. Refract. Metals Hard. Mater.* 110 (2023), <https://doi.org/10.1016/j.ijrmhm.2022.105994>.
- [71] D. Zheng, High-Entropy-Alloy CoFeNiCr Bonded WC-Based Cemented Carbide Prepared by Spark Plasma Sintering, *Metall. Mater. Trans. A* 53 (2022) 2724–2729, <https://doi.org/10.1007/s11661-022-06701-6>.
- [72] Q. Zou, Y. Zhang, Y. Li, J. Xiong, Y. Luo, Tribology Properties of Wc-CoCrNiCuFe Cemented Carbide, *SSRN Electron. J.* (2022), <https://doi.org/10.2139/ssrn.4229728>.
- [73] D. Linder, E. Holmström, S. Norgren, High entropy alloy binders in gradient sintered hardmetal, *Int. J. Refract. Metals Hard. Mater.* 71 (2018) 217–220, <https://doi.org/10.1016/j.ijrmhm.2017.11.030>.
- [74] R. Chen, S. Zheng, R. Zhou, B. Wei, G. Yang, P. Chen, J. Cheng, Development of cemented carbides with CoFeNiCrCu high-entropy alloyed binder prepared by spark plasma sintering, *Int. J. Refract. Metals Hard. Mater.* 103 (2022), <https://doi.org/10.1016/j.ijrmhm.2021.105751>.
- [75] M. Schwarzkopf, H.E. Exner, H.F. Fischmeister, W. Schintlmeister, Kinetics of compositional modification of (W, Ti)C-WC-Co alloy surfaces, *Mater. Sci. Eng.* 105–106 (1988) 225–231, [https://doi.org/10.1016/0025-5416\(88\)90500-9](https://doi.org/10.1016/0025-5416(88)90500-9).
- [76] A. Mueller-Grunz, P. Alveen, S. Rassbach, R. Useldinger, S. Moseley, The manufacture and characterization of WC-(Al)CoCrCuFeNi cemented carbides with nominally high entropy alloy binders, *Int. J. Refract. Metals Hard. Mater.* 84 (2019), <https://doi.org/10.1016/j.ijrmhm.2019.105032>.
- [77] C. Yang, J. Lin, J. Zeng, S. Qu, X. Li, W. Zhang, D. Zhang, High-Strength AlCrFeCoNi High Entropy Alloys Fabricated by Using Metallic Glass Powder as Precursor, *Adv. Eng. Mater.* 18 (2016) 348–353, <https://doi.org/10.1002/adem.201500339>.
- [78] Y.P. Wang, B.S. Li, M.X. Ren, C. Yang, H.Z. Fu, Microstructure and compressive properties of AlCrFeCoNi high entropy alloy, *Mater. Sci. Eng. A* 491 (2008) 154–158, <https://doi.org/10.1016/j.msea.2008.01.064>.
- [79] Y. Zhang, Mechanical properties and structures of high entropy alloys and bulk metallic glasses composites, in: *Materials Science Forum*, Trans Tech Publications Ltd, 2010: pp. 1058–1061. <https://doi.org/10.4028/www.scientific.net/MSF.654-656.1058>.
- [80] C.S. Chen, C.C. Yang, H.Y. Chai, J.W. Yeh, J.L.H. Chau, Novel cermet material of WC/multi-element alloy, *Int. J. Refract. Metals Hard. Mater.* 43 (2014) 200–204, <https://doi.org/10.1016/j.ijrmhm.2013.11.005>.
- [81] W. Luo, Y. Liu, J. Shen, Effects of binders on the microstructures and mechanical properties of ultrafine WC-10%AlxCoCrCuFeNi composites by spark plasma sintering, *J. Alloy. Compd.* 791 (2019) 540–549, <https://doi.org/10.1016/j.jallcom.2019.03.328>.
- [82] C.C. Tung, J.W. Yeh, T. Tsung Shun, S.K. Chen, Y.S. Huang, H.C. Chen, On the elemental effect of AlCoCrCuFeNi high-entropy alloy system, *Mater. Lett.* 61 (2007) 1–5, <https://doi.org/10.1016/j.matlet.2006.03.140>.
- [83] C.W. Li, K.C. Chang, A.C. Yeh, On the microstructure and properties of an advanced cemented carbide system processed by selective laser melting, *J. Alloy. Compd.* 782 (2019) 440–450, <https://doi.org/10.1016/j.jallcom.2018.12.187>.
- [84] W. Luo, Y. Liu, C. Tu, Wetting behaviors and interfacial characteristics of molten AlxCoCrCuFeNi high-entropy alloys on a WC substrate, *J. Mater. Sci. Technol.* 78 (2021) 192–201, <https://doi.org/10.1016/j.jmst.2020.10.067>.
- [85] H. Taimatsu, S. Sugiyama, Y. Kodaira, Synthesis of W2C by reactive hot pressing and its mechanical properties, *Mater. Trans.* 49 (2008) 1256–1261, <https://doi.org/10.2320/matertrans.MRA2007304>.
- [86] S. Yadav, Q. Zhang, A. Behera, R.S. Haridas, P. Agrawal, J. Gong, R.S. Mishra, Role of binder phase on the microstructure and mechanical properties of a mechanically alloyed and spark plasma sintered WC-FCC HEA composites, *J. Alloy. Compd.* 877 (2021), <https://doi.org/10.1016/j.jallcom.2021.160265>.
- [87] W. Luo, Y. Liu, Y. Luo, M. Wu, Fabrication and characterization of WC-AlCoCrCuFeNi high-entropy alloy composites by spark plasma sintering, *J. Alloy. Compd.* 754 (2018) 163–170, <https://doi.org/10.1016/j.jallcom.2018.04.270>.
- [88] R.K. Enneti, K.C. Prough, T.A. Wolfe, A. Klein, N. Studley, J.L. Trasorras, Sintering of WC-12%Co processed by binder jet 3D printing (BJ3DP) technology, *Int. J. Refract. Metals Hard. Mater.* 71 (2018) 28–35, <https://doi.org/10.1016/j.ijrmhm.2017.10.023>.
- [89] Y. Peng, H. Wang, C. Zhao, H. Hu, X. Liu, X. Song, Nanocrystalline WC-Co composite with ultrahigh hardness and toughness, *Compos. B Eng.* 197 (2020), <https://doi.org/10.1016/j.compositesb.2020.108161>.
- [90] T.S. Biurrun, J.N. Cuadrado, U.G. Napal, B.L. Ezquerria, L.L. Cabezas, J. M. Sánchez Moreno, Reactive sintering of WC-Ni-Co-Cr-Ti-Al cemented carbides and precipitation of gamma prime in their metallic binder phases, *Int. J. Refract. Metals Hard. Mater.* 95 (2021), <https://doi.org/10.1016/j.ijrmhm.2020.105427>.
- [91] T. Soria Biurrun, B. Lopez Ezquerria, L. Lozada Cabezas, J.M. Sánchez Moreno, Effect of milling conditions and binder phase content on liquid phase sintering of heat treatable WC-Ni-Co-Cr-Al-Ti cemented carbides, *Int. J. Refract. Metals Hard. Mater.* 88 (2022), <https://doi.org/10.1016/j.ijrmhm.2020.105202>.
- [92] B.L. Ezquerria, T.S. Biurrun, L.L. Cabezas, J.M. Sánchez Moreno, F.J. Lopez, R. M. Pampliega, Sintering of WC hardmetals with Ni-Co-Cr-Ti-Al multi-component alloys, *Int. J. Refract. Metals Hard. Mater.* 77 (2018) 44–53, <https://doi.org/10.1016/j.ijrmhm.2018.07.007>.
- [93] S. Nakonechnyi, A. Yurkova, A. Minitsky, WC-based Cemented Carbides with Nanostructured NiFeCrWMo High-Entropy Alloy Binder, in: *Institute of Electrical and Electronics Engineers (IEEE)*, 2022, pp. 01–05, <https://doi.org/10.1109/nap55339.2022.9934594>.
- [94] D. Kim, Y. Choi, Y. Kim, S. Jung, Characteristics of nanophase WC and WC-3 wt% (Ni Co, and Fe) alloys using a rapid sintering process for the application of friction stir processing tools, *Adv. Mater. Sci. Eng.* 2015 (2015), <https://doi.org/10.1155/2015/343619>.
- [95] Y. Zheng, W. Liu, S. Wang, W. Xiong, Effect of carbon content on the microstructure and mechanical properties of Ti(C, N)-based cermets, *Ceram. Int.* 30 (2004) 2111–2115, <https://doi.org/10.1016/j.ceramint.2003.11.016>.
- [96] A. Rajabi, M.J. Ghazali, A.R. Daud, Chemical composition, microstructure and sintering temperature modifications on mechanical properties of TiC-based cermet - a review, *Mater. Des.* 67 (2015) 95–106, <https://doi.org/10.1016/j.matdes.2014.10.081>.
- [97] Y. Peng, H. Miao, Z. Peng, Development of TiCN-based cermets: Mechanical properties and wear mechanism, *Int. J. Refract. Metals Hard. Mater.* 39 (2013) 78–89, <https://doi.org/10.1016/j.ijrmhm.2012.07.001>.
- [98] P. Ettmayer, H. Kolaska, Ti (C, N) cermets—metallurgy and properties, *Int. J. Refract. Metals Hard. Mater.* 13 (1995) 343–351, [https://doi.org/10.1016/0263-4368\(95\)00027-G](https://doi.org/10.1016/0263-4368(95)00027-G).

- [99] S. Zhang, Titanium carbonitride-based cermets: processes and properties, *Mater. Sci. Eng. A* 163 (1993) 141–148, [https://doi.org/10.1016/0921-5093\(93\)90588-6](https://doi.org/10.1016/0921-5093(93)90588-6).
- [100] M. Shimada, T. Suzuki, M. Koizumi, Fabrication and characterization of $TiC_{1-x}N_x$ ($0 \leq x \leq 1$) and $Mo_2B_2-xC_x$ ($x = 0, 1.0, 2.0$) by high-pressure hot-pressing, *Mater Lett* 1 (1983) 175–177, [https://doi.org/10.1016/0167-577X\(83\)90011-3](https://doi.org/10.1016/0167-577X(83)90011-3).
- [101] S. Cardinal, A. Malchère, V. Garnier, G. Fantozzi, Microstructure and mechanical properties of TiC-TiN based cermets for tools application, *Int. J. Refract. Metals Hard. Mater.* 27 (2009) 521–527, <https://doi.org/10.1016/j.jrmhm.2008.10.006>.
- [102] M. Humenik, N.M. Parikh, Cermets: I, fundamental concepts related to microstructure and physical properties of cermet systems, *J. Am. Ceram. Soc.* 39 (1956) 60–63, <https://doi.org/10.1111/j.1151-2916.1956.tb15624.x>.
- [103] D. Moskowitz, M. Humenik, Cemented titanium carbide cutting tools, *Modern Developments in Powder Metallurgy* (1966) 83–94, https://doi.org/10.1007/978-1-4684-7712-2_6.
- [104] J. Russias, S. Cardinal, Y. Aguni, G. Fantozzi, K. Bienvenu, J. Fontaine, Influence of titanium nitride addition on the microstructure and mechanical properties of TiC-based cermets, *Int. J. Refract. Metals Hard. Mater.* 23 (2005) 358–362, <https://doi.org/10.1016/j.jrmhm.2005.05.008>.
- [105] J. Zackrisson, H.-O. André, Effect of carbon content on the microstructure and mechanical properties of (Ti, W, Ta, Mo)(C, N)-(Co, Ni) cermets, *Int. J. Refract. Metals Hard. Mater.* 17 (1999) 265–273, [https://doi.org/10.1016/S0263-4368\(98\)00074-2](https://doi.org/10.1016/S0263-4368(98)00074-2).
- [106] W. Lengauer, F. Scagnetto, Ti(C, N)-based cermets: Critical review of achievements and recent developments, *Solid State Phenom.* 274 (2018) 53–100, <https://doi.org/10.4028/www.scientific.net/SSP.274.53>.
- [107] P. Lindahl, A.E. Rosén, P. Gustafson, U. Rolander, H.O. André, Effect of pre-alloyed raw materials on the microstructure of a (Ti, W)(C, N)-Co cermet, *Int. J. Refract. Metals Hard. Mater.* 18 (2000) 273–279, [https://doi.org/10.1016/S0263-4368\(00\)00029-9](https://doi.org/10.1016/S0263-4368(00)00029-9).
- [108] A. Aramian, Z. Sadeghian, M. Narimani, N. Razavi, F. Berto, A review on the microstructure and properties of TiC and Ti(C, N) based cermets, *Int. J. Refract. Metals Hard. Mater.* 115 (2023), <https://doi.org/10.1016/j.jrmhm.2023.106320>.
- [109] H. Xiong, Z. you Li, X. Gan, L. Chai, Morphology evolution of TiC-based cermets via different sintering schedules, *Ceram. Int.* 43 (2017) 5805–5812, <https://doi.org/10.1016/j.ceramint.2017.01.133>.
- [110] Q. Liu, G. Wang, X. Sui, Y. Xu, Y. Liu, J. Yang, Ultra-fine grain Ti_xVnBmTa refractory high-entropy alloys with superior mechanical properties fabricated by powder metallurgy, *J. Alloy. Compd.* 865 (2021), <https://doi.org/10.1016/j.jallcom.2020.158592>.
- [111] O.N. Senkov, G.B. Wilks, D.B. Miracle, C.P. Chuang, P.K. Liaw, Refractory high-entropy alloys, *Intermetallics (barking)* 18 (2010) 1758–1765, <https://doi.org/10.1016/j.intermet.2010.05.014>.
- [112] A.S. Rogachev, S.G. Vadchenko, N.A. Kochetov, D.Y. Kovalev, I.D. Kovalev, A. S. Shchukin, A.N. Gryadunov, F. Baras, O. Politano, Combustion synthesis of TiC-based ceramic-metal composites with high entropy alloy binder, *J. Eur. Ceram. Soc.* 40 (2020) 2527–2532, <https://doi.org/10.1016/j.jeurceramsoc.2019.11.059>.
- [113] A.S. Rogachev, A.N. Gryadunov, N.A. Kochetov, A.S. Schukin, F. Baras, O. Politano, High-Entropy-Alloy Binder for TiC-Based Cemented Carbide by SHS Method, *Int. J. Self-Propagating High-Temperature Synth.* 28 (2019) 196–198, <https://doi.org/10.3103/S1061386219030117>.
- [114] A.G. de la Obra, M.J. Sayagués, E. Chicardi, F.J. Gotor, Development of Ti(C, N)-based cermets with (Co, Fe, Ni)-based high entropy alloys as binder phase, *J. Alloy. Compd.* 814 (2020), <https://doi.org/10.1016/j.jallcom.2019.152218>.
- [115] A.G. de la Obra, M.A. Avilés, Y. Torres, E. Chicardi, F.J. Gotor, A new family of cermets: Chemically complex but microstructurally simple, *Int. J. Refract. Metals Hard. Mater.* 63 (2017) 17–25, <https://doi.org/10.1016/j.jrmhm.2016.04.011>.
- [116] C. Real, M.D. Alcalá, I. Trigo, I. Fombella, J.M. Córdoba, Fabrication and characterization of FeCoNiCrMn_(Al) high entropy alloy based (Ti, Ta, Nb)(C, N) cermet, *Int. J. Refract. Metals Hard. Mater.* 101 (2021) 105694, <https://doi.org/10.1016/j.jrmhm.2021.105694>.
- [117] C.-M. Lin, C.-W. Tsai, S.-M. Huang, C.-C. Yang, J.-W. Yeh, New TiC/Co_{1.5}CrFeNi_{1.5}Ti_{0.5} Cermet with Slow TiC Coarsening During Sintering, *JOM* 66 (2014) 2050–2056, <https://doi.org/10.1007/s11837-014-1095-8>.
- [118] Z. Li, C. Zhu, B. Cai, F. Chang, X. Liu, M.Z. Naem, P. Dai, Effect of TiB₂ content on the microstructure and mechanical properties of Ti(C, N)TiB₂FeCoCrNiAl high-entropy alloys composite cermets, *J. Ceram. Soc. Jpn.* 128 (2020) 66–74, <https://doi.org/10.2109/jcersj2.19154>.
- [119] Z.W. He, M.Z. Wang, X.L. Hao, Q. Zou, Y.C. Zhao, Novel cemented carbide produced with TiN_{0.3} and high-entropy alloys, *Rare Met.* 36 (2017) 494–500, <https://doi.org/10.1007/s12598-017-0921-x>.
- [120] Z. Li, X. Liu, K. Guo, H. Wang, B. Cai, F. Chang, C. Hong, P. Dai, Microstructure and properties of Ti(C, N)-TiB₂-FeCoCrNiAl high-entropy alloys composite cermets, *Mater. Sci. Eng. A* 767 (2019) 138427, <https://doi.org/10.1016/j.msea.2019.138427>.
- [121] Z. Wang, J. Xiong, Z. Guo, T. Yang, J. Liu, B. Chai, The microstructure and properties of novel Ti(C, N)-based cermets with multi-component CoCrFeNiCu high-entropy alloy binders, *Mater. Sci. Eng. A* 766 (2019) 138345, <https://doi.org/10.1016/j.msea.2019.138345>.
- [122] B. Chai, J. Xiong, Z. Guo, J. Liu, L. Ni, Y. Xiao, C. Chen, Structure and high temperature wear characteristics of CVD coating on HEA-bonded cermet, *Ceram. Int.* 45 (2019) 19077–19085, <https://doi.org/10.1016/j.ceramint.2019.06.152>.
- [123] S. Yang, J. Xiong, Z. Guo, B. Wu, T. Yang, Q. You, J. Liu, C. Deng, D. Fang, S. Gou, Z. Yu, S. Chen, Effects of CrMnFeCoNi additions on microstructure, mechanical properties and wear resistance of Ti(C, N)-based cermets, *J. Mater. Res. Technol.* 17 (2022) 2480–2494, <https://doi.org/10.1016/j.jmrt.2022.02.021>.
- [124] Y. Fang, N. Chen, G. Du, M. Zhang, X. Zhao, H. Cheng, J. Wu, High-temperature oxidation resistance, mechanical and wear resistance properties of Ti(C, N)-based cermets with Al_{0.3}CoCrFeNi high-entropy alloy as a metal binder, *J. Alloys Compd.* 815 (2020) 152486, <https://doi.org/10.1016/j.jallcom.2019.152486>.
- [125] Q. Gou, J. Xiong, Z. Guo, J. Liu, L. Yang, X. Li, Influence of NbC additions on microstructure and wear resistance of Ti(C, N)-based cermets bonded by CoCrFeNi high-entropy alloy, *Int. J. Refract. Metals Hard. Mater.* 94 (2021) 105375, <https://doi.org/10.1016/j.jrmhm.2020.105375>.
- [126] Z. Li, P. Fu, C. Hong, F. Chang, P. Dai, Tribological behavior of Ti(C, N)-TiB₂ composite cermets using FeCoCrNiAl high entropy alloys as binder over a wide range of temperatures, *Mater. Today Commun.* 26 (2021) 102095, <https://doi.org/10.1016/j.mtcomm.2021.102095>.
- [127] J. Liu, Y. Huo, J. Xiong, Z. Guo, T. Yang, J. Ye, J. Zhao, Y. Liu, Growth and properties of multi-layer nano CrAlN/TiAlN composite coating on the cermets with CrFeCoNiMo, CrFeCoNiMn, CrFeCoNiAl High Entropy Alloy Phase, *Appl Surf Sci* 572 (2022) 151309, <https://doi.org/10.1016/j.apsusc.2021.151309>.
- [128] G. Zhu, Y. Liu, J. Ye, Fabrication and properties of Ti(C, N)-based cermets with multi-component AlCoCrFeNi high-entropy alloys binder, *Mater. Lett.* 113 (2013) 80–82, <https://doi.org/10.1016/j.matlet.2013.08.087>.
- [129] G. Zhu, Y. Liu, J. Ye, Early high-temperature oxidation behavior of Ti(C, N)-based cermets with multi-component AlCoCrFeNi high-entropy alloy binder, *Int. J. Refract. Metals Hard. Mater.* 44 (2014) 35–41, <https://doi.org/10.1016/j.jrmhm.2014.01.005>.
- [130] R.G. Munro, Material properties of titanium diboride, *J. Res. Nat. Inst. Stand. Technol.* 105 (2000) 709, <https://doi.org/10.6028/jres.105.057>.
- [131] V.I. Matkovich, Boron and Refractory Borides (1977), <https://doi.org/10.1007/978-3-642-66620-9>.
- [132] F. De Mestral, F. Thevenot, Ceramic composites: TiB₂-TiC-SiC Part I Properties and microstructures in the ternary system, *J. Mater. Sci.* 26 (1991) 5547–5560, <https://doi.org/10.1007/BF00553658>.
- [133] S. Baik, P.F. Becher, Effect of Oxygen Contamination on Densification of TiB₂, *J. Am. Ceram. Soc.* 70 (1987) 527–530, <https://doi.org/10.1111/j.1151-2916.1987.tb05699.x>.
- [134] C. Yang, H. Guo, D. Mo, S. Qu, X. Li, W. Zhang, L. Zhang, Bulk TiB₂-Based Ceramic Composites with Improved Mechanical Property Using Fe-Ni-Ti-Al as a Sintering Aid, *Materials* 7 (2014) 7105–7117, <https://doi.org/10.3390/ma7107105>.
- [135] Y. Yang, B. Yin, Y. Shang, X. Wang, J. Chen, Preparation and characterization of novel TiB₂-12 (Fe-Co-Cr-Ni) cermets and their corrosion resistance in molten aluminum, *Corros. Sci.* 190 (2021) 109643, <https://doi.org/10.1016/j.corsci.2021.109643>.
- [136] Z.H. Zhang, X.B. Shen, F.C. Wang, S.K. Lee, L. Wang, Densification behavior and mechanical properties of the spark plasma sintered monolithic TiB₂ ceramics, *Mater. Sci. Eng. A* 527 (2010) 5947–5951, <https://doi.org/10.1016/j.msea.2010.05.086>.
- [137] J.M. Sánchez, I. Azcona, F. Castro, Mechanical properties of titanium diboride based cermets, *J. Mater. Sci.* 35 (2000) 9–14, <https://doi.org/10.1023/A:1004763709854>.
- [138] S. Zhang, Y. Sun, B. Ke, Y. Li, W. Ji, W. Wang, Z. Fu, Preparation and characterization of TiB₂-(supra-nano-dual-phase) high-entropy alloy cermet by spark plasma sintering, *Metals (basel)* 8 (2018), <https://doi.org/10.3390/met8010058>.
- [139] Y. Li, H. Xu, B. Ke, Y. Sun, K. Yang, W. Ji, W. Wang, Z. Fu, TEM characterization of a Supra-Nano-Dual-Phase binder phase in spark plasma sintered TiB₂-5 wt% HEAs cermet, *Ceram. Int.* 45 (2019) 9401–9405, <https://doi.org/10.1016/j.ceramint.2018.08.174>.
- [140] M.G. Barandika, J.M. Sánchez, T. Rojo, R. Cortés, F. Castro, Fe-Ni-Ti binder phases for TiB₂-based cermets: A thermodynamic approach, *Scr. Mater.* 39 (1998) 1395–1400, [https://doi.org/10.1016/S1359-6462\(98\)00312-1](https://doi.org/10.1016/S1359-6462(98)00312-1).
- [141] W. Ji, J. Zhang, W. Wang, H. Wang, F. Zhang, Y. Wang, Z. Fu, Fabrication and properties of TiB₂-based cermets by spark plasma sintering with CoCrFeNiTiAl high-entropy alloy as sintering aid, *J. Eur. Ceram. Soc.* 35 (2015) 879–886, <https://doi.org/10.1016/j.jeurceramsoc.2014.10.024>.
- [142] Z. Fu, R. Koc, Ultrafine TiB₂-TiNiFeCrCoAl high-entropy alloy composite with enhanced mechanical properties, *Mater. Sci. Eng. A* 702 (2017) 184–188, <https://doi.org/10.1016/j.msea.2017.07.008>.
- [143] Z. Fu, R. Koc, Processing and characterization of TiB₂-TiNiFeCrCoAl high-entropy alloy composite, *J. Am. Ceram. Soc.* 100 (2016) 2803–2813, <https://doi.org/10.1111/jace.14814>.
- [144] L.H. Li, H.E. Kim, E. Son Kang, Sintering and mechanical properties of titanium diboride with aluminum nitride as a sintering aid, *J. Eur. Ceram. Soc.* 22 (2002) 973–977, [https://doi.org/10.1016/S0955-2219\(01\)00403-4](https://doi.org/10.1016/S0955-2219(01)00403-4).
- [145] Z.H. Zhang, X.B. Shen, F.C. Wang, S.K. Lee, Q.B. Fan, M.S. Cao, Low-temperature densification of TiB₂ ceramic by the spark plasma sintering process with Ti as a sintering aid, *Scr. Mater.* 66 (2012) 167–170, <https://doi.org/10.1016/j.scriptamat.2011.10.030>.
- [146] K. Zhao, B. Niu, F. Zhang, J. Zhang, Microstructure and mechanical properties of spark plasma sintered TiB₂ ceramics combined with a high-entropy alloy sintering aid, *Adv. Appl. Ceram.* 116 (2016) 19–23, <https://doi.org/10.1080/17436753.2016.1207944>.

- [147] J.P. Guha, D. Kolar, Systems of niobium monocarbide with transition metals, *J. Less-Common Met.* 29 (1972), [https://doi.org/10.1016/0022-5088\(72\)90145-2](https://doi.org/10.1016/0022-5088(72)90145-2).
- [148] H.O. Pierson, *Handbook of refractory carbides and nitrides : properties, characteristics, processing, and applications, Handbook of Refractory Carbides and Nitrides* (1996).
- [149] M. Woydt, H. Mohrbacher, The tribological and mechanical properties of niobium carbides (NbC) bonded with cobalt or Fe₃Al, *Wear* 321 (2014) 1–7, <https://doi.org/10.1016/j.wear.2014.09.007>.
- [150] L. Lanier, G. Metauer, M. Moukassi, Microprecipitation in boron-containing high-carbon steels, *Mikrochim. Acta* 114 (115) (1994) 353–361, <https://doi.org/10.1007/BF01244562>.
- [151] S. Sen, I. Ozbek, U. Sen, C. Bindal, Mechanical behavior of borides formed on borided cold work tool steel, *Surf. Coat. Technol.* 135 (2001) 173–177, [https://doi.org/10.1016/S0257-8972\(00\)01064-1](https://doi.org/10.1016/S0257-8972(00)01064-1).
- [152] Y. Ohishi, M. Sugizaki, Y. Sun, H. Muta, K. Kurosaki, Thermophysical and mechanical properties of CrB and FeB, *J. Nucl. Sci. Technol.* 56 (2019) 859–865, <https://doi.org/10.1080/00223131.2019.1593893>.
- [153] Y. Shao, Z. Guo, Y. Wang, H. Ma, Fabrication and characterization of NbC-CoCrFeNiMn high-entropy alloy cermet, *Int. J. Refract. Metals Hard. Mater.* 94 (2021) 105388, <https://doi.org/10.1016/j.ijrmhm.2020.105388>.
- [154] R. Warren, Carbide grain growth during the liquid-phase sintering of the alloys NbCF_e, NbCNi, and NbCCo, *J. Less-Common Met.* 17 (1969), [https://doi.org/10.1016/0022-5088\(69\)90037-X](https://doi.org/10.1016/0022-5088(69)90037-X).
- [155] W. Zeng, J. Xie, D. Zhou, Z. Fu, D. Zhang, E.J. Laverna, In-situ formation of NbC in nanocrystalline Cu, *J. Alloy. Compd.* 725 (2017), <https://doi.org/10.1016/j.jallcom.2017.07.179>.
- [156] X. Xie, B. Yin, Y. Yang, X. Wang, F. Yin, Corrosion Resistance to Molten Zinc of a Novel FeB-10 Mo-12 Al_{0.25}FeNiCoCr Cermet and Coating, *J. Therm. Spray Technol.* 31 (2022) 1423–1438, <https://doi.org/10.1007/s11666-021-01283-y>.
- [157] X. Xie, B. Yin, F. Yin, X. Ouyang, Corrosion behavior of FeB-30 wt.% Al_{0.25}FeNiCoCr Cermet Coating in Liquid Zinc, *Coatings* 6 (2021) 622, <https://doi.org/10.3390/coatings11060622>.
- [158] X. Xie, F. Yin, X. Wang, X. Ouyang, M. Li, J. Hu, Corrosion Resistance to Molten Zinc of a Novel Cermet Coating Deposited by Activated Combustion High-Velocity Air Fuel (AC-HVAF), *J. Therm. Spray Technol.* 28 (2019) 1252–1262, <https://doi.org/10.1007/s11666-019-00893-x>.
- [159] S.M.A. Shibli, B.N. Meena, R. Remya, A review on recent approaches in the field of hot dip zinc galvanizing process, *Surf. Coat. Technol.* 262 (2015) 210–215, <https://doi.org/10.1016/j.surfcoat.2014.12.054>.
- [160] D.N. Tsipas, G.K. Triantafyllidis, J.K. Kiplagat, P. Psillaki, Degradation behaviour of boronized carbon and high alloy steels in molten aluminium and zinc, 1998.
- [161] O. Allaoui, N. Bouaouadja, G. Sainderman, Characterization of boronized layers on a XC38 steel, *Surf. Coat. Technol.* 201 (2006) 3475–3482, <https://doi.org/10.1016/j.surfcoat.2006.07.238>.
- [162] O. Ozdemir, M. Usta, C. Bindal, A.H. Ucisik, Hard iron boride (Fe₂B) on 99.97 wt % pure iron, *Vacuum* 80 (2006) 1391–1395, <https://doi.org/10.1016/j.vacuum.2006.01.022>.
- [163] H. Mizuno, J. Kitamura, MoB/CoCr cermet coatings by HVOF spraying against erosion by molten Al-Zn alloy, *J. Therm. Spray Technol.* 16 (2007) 404–413, <https://doi.org/10.1007/s11666-007-9046-3>.
- [164] X. Liu, J. Zhang, C. Hou, H. Wang, X. Song, Z. Nie, Mechanisms of WC plastic deformation in cemented carbide, *Mater. Des.* 150 (2018) 154–164, <https://doi.org/10.1016/J.MATDES.2018.04.025>.
- [165] T. Li, Q. Li, J.Y.H. Fuh, P.C. Yu, L. Lu, C.C. Wu, Effects of AGG on fracture toughness of tungsten carbide, *Mater. Sci. Eng. A* 445–446 (2007) 587–592, <https://doi.org/10.1016/J.MSEA.2006.09.076>.
- [166] T. Bai, T. Xie, Fabrication and mechanical properties of WC-Al₂O₃ cemented carbide reinforced by CNTs, *Mater. Chem. Phys.* 201 (2017) 113–119, <https://doi.org/10.1016/J.MATCHEMPHYS.2017.08.018>.
- [167] B. Zou, C. Huang, J. Song, Z. Liu, L. Liu, Y. Zhao, Mechanical properties and microstructure of TiB₂-TiC composite ceramic cutting tool material, *Int. J. Refract. Metals Hard. Mater.* 35 (2012) 1–9, <https://doi.org/10.1016/J.IJRMHM.2012.02.011>.
- [168] P.F. Becher, Microstructural design of toughened ceramics, *J. Am. Ceram. Soc.* 74 (1991), <https://doi.org/10.1111/j.1151-2916.1991.tb06872.x>.
- [169] L. Kvetková, A. Duszová, P. Hvizdoš, J. Duszka, P. Kun, C. Balázi, Fracture toughness and toughening mechanisms in graphene platelet reinforced Si₃N₄ composites, *Scr. Mater.* 66 (2012) 793–796, <https://doi.org/10.1016/J.SCRIPTAMAT.2012.02.009>.
- [170] J.K. Xiao, H. Tan, Y.Q. Wu, J. Chen, C. Zhang, Microstructure and wear behavior of FeCoNiCrMn high entropy alloy coating deposited by plasma spraying, *Surf. Coat. Technol.* 385 (2020), <https://doi.org/10.1016/j.surfcoat.2020.125430>.
- [171] J. Chu, Y. Bao, Volatilization behavior of manganese from molten steel with different alloying methods in vacuum, *Metals (Basel)* 10 (2020) 1–10, <https://doi.org/10.3390/met10101348>.
- [172] S.G. Park, M.C. Kim, B.S. Lee, D.M. Wee, Correlation of the thermodynamic calculation and the experimental observation of Ni-Mo-Cr low alloy steel changing Ni, Mo, and Cr contents, *J. Nucl. Mater.* 407 (2010) 126–135, <https://doi.org/10.1016/j.jnucmat.2010.09.004>.
- [173] Y. Jianpeng, Y. Yueguang, S. Jie, Cermet composite coating with a ductile Ni₃Al binder phase and an in-situ Cr₇C₃ augmented phase, *Intermetallics (Barking)* 138 (2021) 107300, <https://doi.org/10.1016/J.INTERMET.2021.107300>.
- [174] X. Yan, H. Guo, W. Yang, S.J. Pang, Q. Wang, Y. Liu, P.K. Liaw, T. Zhang, Al_{0.3}Cr_xFeCoNi high-entropy alloys with high corrosion resistance and good mechanical properties, *J. Alloys Compd.* 860 (2021), <https://doi.org/10.1016/j.jallcom.2020.158436>.
- [175] Z. Xu, H. Zhang, X. Du, Y. He, H. Luo, G. Song, L. Mao, T. Zhou, L. Wang, Corrosion resistance enhancement of CoCrFeMnNi high-entropy alloy fabricated by additive manufacturing, *Corros. Sci.* 177 (2020), <https://doi.org/10.1016/j.corsci.2020.108954>.
- [176] R.B. Nair, H.S. Arora, S. Mukherjee, S. Singh, H. Singh, H.S. Grewal, Exceptionally high cavitation erosion and corrosion resistance of a high entropy alloy, *Ultrason. Sonochem.* 41 (2018) 252–260, <https://doi.org/10.1016/j.ultsonch.2017.09.044>.
- [177] Y.C. Ma, X.J. Zhao, M. Gao, K. Liu, High-Temperature Oxidation Behavior of a Ni-Cr-W-Al Alloy, *J. Mater. Sci. Technol.* 27 (2011) 841–845, [https://doi.org/10.1016/S1005-0302\(11\)60152-7](https://doi.org/10.1016/S1005-0302(11)60152-7).
- [178] Y. Fang, L. Xia, G. Chen, T. Wu, R. Wang, X. Yu, K. Chen, M. Zhang, X. Zhao, H. Cheng, High-performance Ti(C, N)-based cermet with ZrO₂ whiskers and Al_{0.3}CoCrFeNi high-entropy alloy, *Int. J. Refract. Metals Hard. Mater.* 109 (2022) 105990, <https://doi.org/10.1016/j.ijrmhm.2022.105990>.
- [179] P. Fu, Z. Li, X. Wen, C. Liu, F. Chang, L. Lin, P. Dai, Effect of high-entropy alloy binder content on the microstructure, mechanical properties and oxidation behavior of Ti(C, N)TiB₂cermets, *J. Ceram. Soc. Jpn.* 129 (2021) 504–515, <https://doi.org/10.2109/jcersj2.21075>.